17. Hutchison AJ, Wilson RJ, Garafola S *et al.* Lanthanum carbonate: safety data after 10 years. *Nephrology* 2016; 21: 987–994
18. Pieper AK, Haffner D, Hoppe B *et al.* A randomized crossover trial comparing sevelamer with calcium acetate in children with CKD. *Am J Kidney Dis* 2006; 47: 625–635
19. Sheikh MS, Maguire JA, Emmett M *et al.* Reduction of dietary phosphorus absorption by phosphorus binders. A theoretical, in vitro, and in vivo study. *J Clin Invest* 1989; 83: 66–73
20. Larsson TE, Kameoka C, Nakajo I *et al.* Npt-IIb inhibition does not improve hyperphosphatemia in CKD. *Kidney Int Rep* 2018; 3: 73–80
21. Aniteli TM, de Siqueira FR, Dos Reis LM *et al.* Effect of variations in dietary Pi intake on intestinal Pi transporters (NaPi-IIb, Pit-1, and Pit-2) and phosphate-regulating factors (PTH, FGF-23, and MEPE). *Pflugers Arch* 2018; 470: 623–632
22. Giral H, Caldas Y, Sutherland E *et al.* Regulation of rat intestinal Na-dependent phosphate transporters by dietary phosphate. *Am J Physiol Renal Physiol* 2009; 297: F1466–F1475
23. Kamiie J, Ohtsuki S, Iwase R *et al.* Quantitative atlas of membrane transporter proteins. Development and application of a highly sensitive simultaneous LC/MS/MS method combined with novel in-silico peptide selection criteria. *Pharm Res* 2008; 25: 1469–1483
24. Cheng QL, Orikasa M, Morioka T *et al.* Progressive renal lesions induced by administration of monoclonal antibody 1-22-3 to unilaterally nephrectomized rats. *Clin Exp Immunol* 2008; 102: 181–185
25. Ichida Y, Hosokawa N, Takemoto R *et al.* Significant species differences in intestinal phosphate absorption between dogs, rats, and monkeys. *J Nutr Sci Vitaminol* 2020; 66: 60–67
26. Takahashi K, Masuda S, Nakamura N *et al.* Upregulation of H^+-peptide cotransporter PEPT2 in rat remnant kidney. *Am J Physiol Renal Physiol* 2001; 281: F1109–F1116
27. Kamiie J, Sumio, O, Tetsuya, T. Method of quantifying membrane protein by using mass spectrometer. *Japan Patent* 2011; 4670060
28. Forster IC, Virkki L, Bossi E *et al.* Electrogenic kinetics of a mammalian intestinal type IIb Na^+/P_i cotransporter. *J Membrane Biol* 2006; 212: 177–190
29. Ravera S, Virkki LV, Murer H *et al.* Deciphering pit transport kinetics and substrate specificity using electrophysiology and flux measurements. *Am J Physiology Cell Physiol* 2007; 293: C606–C620
30. Brown AJ, Zhang F, Ritter CS. The vitamin D analog ED-71 is a potent regulator of intestinal phosphate absorption and NaPi-IIb. *Endocrinology* 2012; 153: 5150–5156
31. Hattenhauer O, Traebert M, Murer H *et al.* Regulation of small intestinal Na-P_i type IIb cotransporter by dietary phosphate intake. *Am J Physiol* 1999; 277: G756–G762
32. Segawa H, Kaneko I, Yamanaka S *et al.* Intestinal Na-P_i cotransporter adaptation to dietary P_i content in vitamin D receptor null mice. *Am J Physiol Renal Physiol* 2004; 287: F39–F47
33. Katsumata K, Kusano K, Hirata M *et al.* Sevelamer hydrochloride prevents ectopic calcification and renal osteodystrophy in chronic renal failure rats. *Kidney Int* 2003; 64: 441–450
34. Tsuboi Y, Ohtomo S, Ichida Y *et al.* EOS789, a novel inhibitor of multi-phosphate transporters, is effective for the treatment of chronic kidney disease–mineral bone disorder ilure rats. *Kidney Int* 2020; 10.1016/j.kint.2020.02.040

Received: 28.2.2020; Editorial decision: 13.5.2020

Nephrol Dial Transplant (2021) 36: 75–86
doi: 10.1093/ndt/gfaa223
Advance Access publication 25 October 2020

Aberrant mucosal immunoreaction to tonsillar microbiota in immunoglobulin A nephropathy

Hiroki Yamaguchi[1], Shin Goto[1], Nao Takahashi[2], Masafumi Tsuchida[1], Hirofumi Watanabe[1], Suguru Yamamoto[1], Yoshikatsu Kaneko[1], Koichi Higashi[3], Hiroshi Mori[3], Yukio Nakamura[4], Arata Horii[2], Ken Kurokawa[3] and Ichiei Narita[1]

[1]Division of Clinical Nephrology and Rheumatology, Kidney Research Center, Niigata University Graduate School of Medical and Dental Sciences, Niigata, Japan, [2]Department of Otolaryngology Head and Neck Surgery, Niigata University Graduate School of Medical and Dental Sciences, Niigata, Japan, [3]Genome Evolution Laboratory, National Institute of Genetics, Mishima, Japan and [4]Repertoire Genesis Incorporation, Ibaraki, Japan

Correspondence to: Shin Goto; E-mail: gotos@med.niigata-u.ac.jp

ABSTRACT

Background. Immunoglobulin A nephropathy (IgAN) is the most common glomerulonephritis worldwide, characterized by mesangial polymeric IgA1 deposition. IgAN is believed to develop owing to aberrant mucosal immunoreaction against commensals in the tonsils. However, the exact interrelation between pathogenic IgA and mucosal microbiota in IgAN patients is unclear.

KEY LEARNING POINTS

What is already known about this subject?

- The interplay between mucosal immunity and microbiota in patients with IgA nephropathy is considered to underlie disease pathogenesis.
- Tonsillectomy has beneficial effects on clinical outcomes of patients with IgA nephropathy.
- We conducted this study to elucidate the mechanisms underlying the mucosal immune response to microbiota at the tonsillar crypts and its role in the development of IgA nephropathy

What this study adds?

- Both a proliferation-inducing ligand and B-cell activating factor expression in tonsillar crypts were elevated in patients with IgA nephropathy, correlating with the expression of immunoglobulin heavy variable 3–30 (IGHV3-30) and IGHV3-38 repertoire, respectively, in IgA1 at the tonsillar crypts.
- Bacteria from the phylum *Bacteroidetes* were highly coated with IgA at the tonsillar crypts of IgA nephropathy patients, correlating with the tonsillar expression of IGHV3-30 in IgA1.
- Serum polymeric IgA, comprising high levels of galactose-deficient IgA1, exhibited considerable binding to *Bacteroidetes* strains cultured from the tonsils of IgA nephropathy patients.

What impact this may have on practice or policy?

- This study strengthens the role of the mucosal immune response to microbiota in the pathogenesis of IgA nephropathy.
- Aberrant mucosal immunoreactions against the host tonsillar microbiota are potentially novel therapeutic targets for the management of IgA nephropathy.

Methods. Biopsy-proven IgAN or recurrent tonsillitis (RT) patients who had undergone tonsillectomy were enrolled. We used 16S ribosomal RNA gene amplicon sequencing with a flow cytometry-based bacterial cell sorting technique) and immunoglobulin repertoire sequencing of the IgA heavy chain to characterize IgA-coated bacteria of the tonsillar microbiota (IgA-SEQ) and their corresponding IgA repertoire. Furthermore, we fractionated patient serum using gel-filtration chromatography and performed flow cytometry-based analysis of IgA binding to bacteria cultured from incised tonsils.

Results. Tonsillar proliferation-inducing ligand and B-cell activating factor levels were significantly higher in IgAN than in RT patients. IgA-SEQ for tonsillar microbiota revealed the preferential binding ability of IgA to *Bacteroidetes* in IgAN tonsils compared with those from RT patients. Expression of immunoglobulin heavy (IGH) constant alpha 1 with IGH variable 3–30 was significantly higher in IgAN than that in RT, and positively correlated with the IgA-coated enrichment score of *Bacteroidetes*. Serum polymeric IgA, comprising high levels of GdIgA1, exhibited considerable binding to *Bacteroidetes* strains cultured from the tonsils of IgAN patients.

Conclusions. These findings provide evidence that aberrant mucosal immune responses to tonsillar anaerobic microbiota, primarily consisting of members of the phylum *Bacteroidetes*, are involved in IgAN pathophysiology.

Keywords: APRIL, IgA nephropathy, immunoglobulin repertoire sequencing, microbiome, tonsillectomy

INTRODUCTION

Immunoglobulin A nephropathy (IgAN) is the most common chronic glomerular disease worldwide and is a major cause of end-stage kidney disease. It is predominantly characterized by pathological IgA1 deposits in the mesangium [1]. Mucosal infections such as tonsillitis and upper respiratory tract infections exacerbate hematuria in IgAN patients. Tonsillectomy, combined with steroid pulse therapy, is therefore widely performed in Japan [2] and has beneficial effects for IgAN clinical remission [3]. Additionally, genome-wide association studies for IgAN have indicated several loci to be involved in regulating mucosal IgA production and innate immunity [4], highlighting the importance of identifying the link between mucosal immunoreaction and IgAN pathogenesis [5].

Mesangial IgA deposits in IgAN patients are predominantly polymeric, aberrantly glycosylated [6, 7], and associated with the J-chain [8], which is preferentially produced by mucosal immunocytes [9]. The bacterial DNA-activated [10] expression of Toll-like receptor (TLR) 9 in the tonsils has also been associated with IgAN progression [11]. Repeated TLR9 activation induces tonsillar expression of a proliferation-inducing ligand (APRIL), which is predominantly produced by dendritic cells [12] and promotes class switching through T-cell-independent immune interactions with commensal microbiota [13–15]. Notably, APRIL expression in patients with an aberrant tonsillar germinal center was responsive to tonsillectomy, exhibiting decreased galactose-deficient IgA1 (GdIgA1) in serum [16]. Although tonsillar mucosal immune dysregulation in IgAN has been thoroughly investigated, the mechanisms underlying pathogenic tonsillar IgA1 production remain unclear.

Previously, we performed high-throughput 16S ribosomal RNA (rRNA) gene sequencing to explore the association of IgAN with bacterial flora in the palatine tonsils [17], but no significant difference was identified in the relative abundance of any bacterial genus between IgAN or recurrent tonsillitis (RT) cases. Recent studies demonstrated that microbiota-induced mucosal IgAs coated diverse microbial antigens [18] and agglutinated their cross-reactive bacterial targets, preventing direct host interaction [19, 20]. Further, bacterial flow cytometry with high-throughput 16S rRNA gene sequencing (IgA-SEQ) characterized IgA-coated microbiota [18, 21]. IgA-SEQ application in fecal samples from mouse and human disease models revealed the roles of IgA-coated intestinal microbiota in

inflammatory bowel disease development [21, 22], indicating that IgA-SEQ could be used to identify disease-related microbes. Furthermore, analyzing peripheral tissue or blood samples using recently developed high-throughput sequencing strategies enabled comprehensive exploration of human immunoglobulin repertoires [23, 24]. Diversification of immunoglobulins, which comprise paired immunoglobulin heavy (IGH) and light chains and constitute the soluble forms of B-cell receptors, is determined via immunoglobulin variable (V), diversity (D) and joining (J) gene segment recombination [25] and subsequent somatic hypermutation [26]. This reveals that microbial symbionts influence host immunity and regulate pre-immune B-cell repertoires independently of T cells [27].

This study aimed to investigate the mucosal immune responses to microbiota in the tonsils of IgAN patients by this multiomics approach using tonsillectomy samples. We also evaluated whether such responses are involved in disease pathology.

MATERIALS AND METHODS

Study population and sample collection

The study protocol adhered to the Declaration of Helsinki and was approved by the Ethics Committee on Genetic Analysis of Niigata University, Niigata, Japan (approval no. G2017-0004). Written informed consent was obtained from all patients. We collected tonsillar samples from IgAN and RT patients who had undergone tonsillectomy from July 2012 to June 2018. IgAN pathological diagnoses and tonsillar sample collection procedures were previously described [17].

Tonsillar protein extraction and enzyme-linked immunosorbent assay

Tonsillar tissue (30 mg) was suspended in T-PER tissue protein extraction reagent (Thermo Scientific, Waltham, MA, USA) and homogenized using the FastPrep®24 mechanical disruptor (MP Biomedicals, Tokyo, Japan) containing ceramic beads, setting the final concentration at 1.0 mg/dL, per bicinchoninic acid assay methods. Serum and tonsil APRIL, B-cell activating factor (BAFF), GdIgA1 and IgA protein concentrations were measured using enzyme-linked immunosorbent assay (ELISA). IgA–IgG complex levels in fractionated serum were also determined by ELISA, as previously reported [28].

Immunostaining

Paraffin-embedded kidney biopsy and incised tonsil sections from enrolled patients were used for immunohistochemistry. After antigen retrieval and blocking, slides were incubated with mouse anti-APRIL/TNFSF13 monoclonal antibody (Aprily-8; Novus Biologicals, Littleton, CO, USA), rat anti-human BAFF monoclonal antibody (Buffy-2; Abcam, Cambridge, UK) antibodies or rat anti-GdIgA1 (KM55; Immuno-Biological Laboratories, Gunma, Japan) [29]. Slides were subsequently incubated with secondary antibodies, as described in the Supplementary data. The proportion of the area stained by immunofluorescence examination with anti-GdIgA1 antibody was quantified to evaluate glomerular GdIgA1 deposition, as per previous studies [8, 30, 31].

Table 1. Characteristics of enrolled patients

Patient characteristics	IgAN ($n = 62$)	RT ($n = 28$)	P-value
Age (years)	32.8 ± 10.3	30.5 ± 9.5	0.361
Sex (male)	26 (41.9)	18 (64.3)	0.069
BMI (kg/m^2)	21.9 ± 2.8	22.6 ± 4.4	0.353
Systolic BP (mmHg)	116.6 ± 13.6	116.2 ± 13.8	0.908
Diastolic BP (mmHg)	71.0 ± 10.1	69.0 ± 9.4	0.407
s-Cre (mg/dL)	0.85 ± 0.27	0.73 ± 0.15	0.052
eGFR (mL/min/1.73 m^2)	80.5 ± 20.5	97.2 ± 19.4	0.001
BUN (mg/mL)	13.7 ± 4.4	12.5 ± 3.2	0.225
TP (g/dL)	7.1 ± 0.5	7.4 ± 0.5	0.054
UA (mg/dL)	5.2 ± 1.4	5.5 ± 1.5	0.678
IgA (mg/dL)	310.8 ± 155.5	–	–
C3 (mg/dL)	95.5 ± 17.5	–	–
Urinary protein (g/day)	0.45 (0.29, 0.90)	–	–
Period from renal biopsy to tonsillectomy (day)	174 (115, 367)	–	–
RASI	39 (62.9)	1 (3.6)	<0.001
Oxford classification			
Mesangial hypercellularity (M0/M1)	49/13		
Endocapillary hypercellularity (E0/E1)	28/34		
Segmental glomerulosclerosis (S0/S1)	14/48		
Tubular atrophy/interstitial fibrosis (T0/T1/T2)	57/5/0		
Crescents (C0/C1/C2)	23/39/0		

Data are presented as the means ± SD, median (IQR) or number (ratio), and were statistically compared using Student's *t*-test or Fisher's exact test. Among the clinical characteristics of these patients, a significant difference was noted in the eGFR and RASI. BMI, body mass index; BP, blood pressure; s-Cre, serum creatinine; eGFR, estimated glomerular filtration rate; BUN, blood urea nitrogen; IQR, interquartile range; TP, total protein; UA, uric acid; C3, complement component 3; RASI, renin–angiotensin–aldosterone system inhibitor.

Bacterial sorting for IgA-SEQ and 16S rRNA gene amplicon sequencing

Bacterial sorting was performed as previously reported [21] and applied to tonsillar samples with some modifications. Briefly, washed bacterial pellets of tonsillar samples were stained with phycoerythrin (PE)-conjugated mouse anti-human IgA (IS11-8E10, Miltenyi Biotec, Bergisch-Gladbach, Germany) or mouse IgG1-PE isotype (Presort sample). The IgA-PE positive fraction enriched and separated by magnetic-activated cell sorting was sorted by fluorescence-activated cell sorting (FACS) to purify the IgA-positive (IgA^+) and IgA-negative (IgA^-) fractions. Details of the 16S rRNA gene amplification sequencing of genomic DNA from tonsillar crypts and sorted fractions are provided in the Supplementary Methods. The IgA index was calculated using the relative abundance of bacterial phyla and genera for IgA^+ and IgA^- fractions as per $[\log(IgA^+) - \log(IgA^-)]/[\log(IgA^+) + \log(IgA^-)]$, as reported previously [22, 32]. The 16S rRNA gene amplicon sequence data were deposited in DDBJ DRA with BioProject ID PRJDB8009.

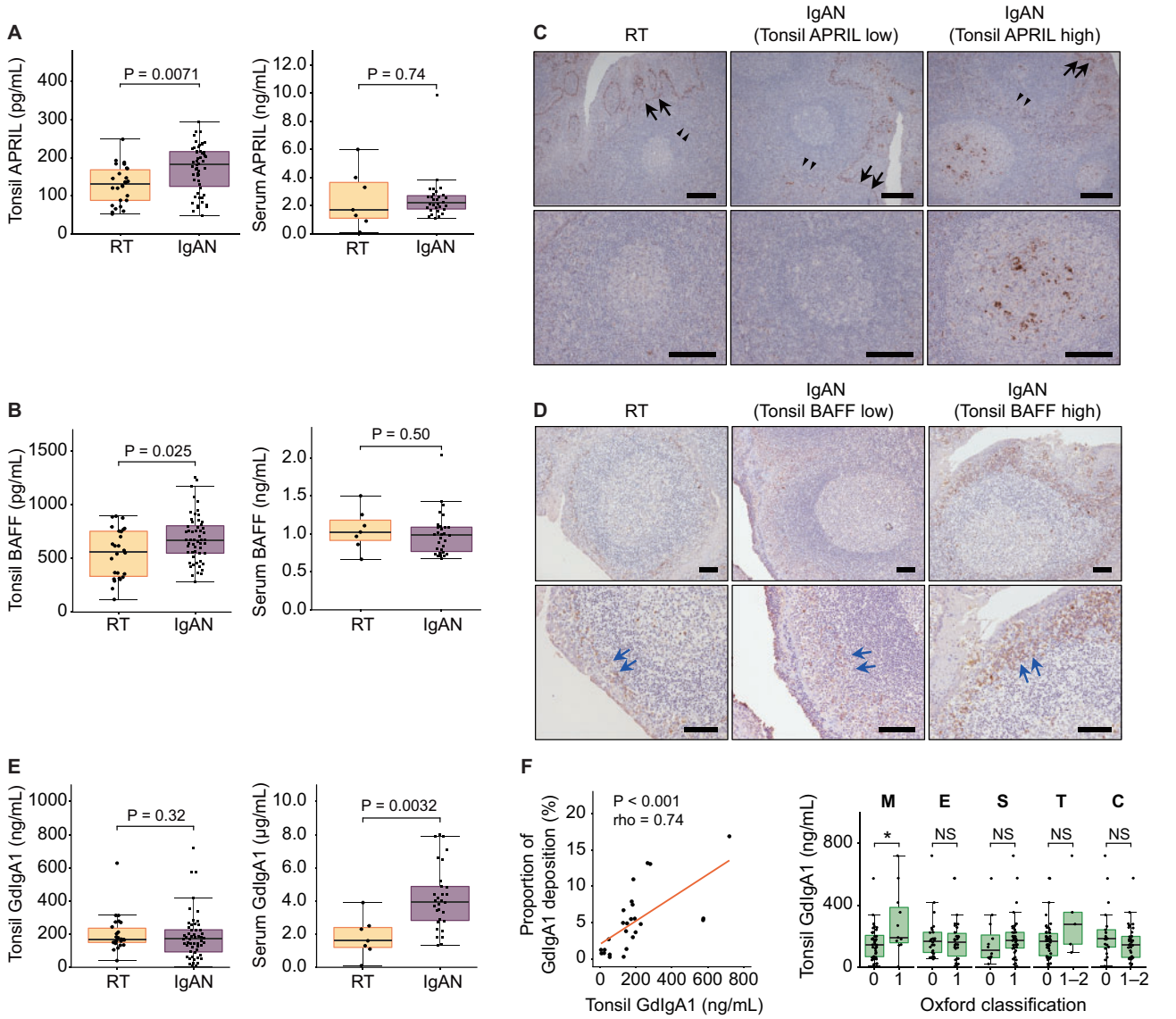

FIGURE 1: Quantification of APRIL, BAFF and GdIgA1 in the tonsillar crypts. APRIL (**A**) and BAFF (**B**) levels of adjusted tonsillar protein solution from IgAN ($n = 55$) and RT patients ($n = 26$) (left) and serum APRIL and BAFF levels from IgAN ($n = 30$) and RT ($n = 7$) (right) patients, respectively. Box plots show the median and interquartile range (IQR), with whiskers of 1.5 × IQR. Data were statistically compared using the Mann–Whitney U test. Immunohistochemistry with an anti-APRIL (**C**) and anti-BAFF (**D**) monoclonal antibody in tonsils from patients with RT (left panels, tonsillar levels of APRIL = 145.3 pg/mL, BAFF = 355.4 pg/mL, respectively), IgAN with low tonsillar APRIL levels (middle panels, levels of APRIL = 128.9 pg/mL, BAFF = 555.1 pg/mL, respectively) and high tonsillar APRIL or BAFF levels (right panels, levels of APRIL = 267.5 pg/mL, BAFF = 1028.2 pg/mL, respectively). Black arrows indicate APRIL staining in basal cells of the surface epithelium. Black arrowheads indicate APRIL staining of perifollicular area. Blue arrows indicate BAFF staining in mantle and perifollicular zone around crypts. Photographs show germinal centers and epithelium around crypts (upper panels; low magnification images, bottom panels; high magnification images). Scale bars: 100 μm. (**E**) GdIgA1 levels of adjusted tonsillar protein solution from IgAN ($n = 55$) and RT patients ($n = 26$) (left) and serum levels of GdIgA1 from IgAN patients ($n = 30$) and RT ($n = 7$) (right), respectively. Box plots show the median and IQR, with whiskers of 1.5 × IQR. Data were statistically compared using the Mann–Whitney U test. (**F**) Correlation between levels of tonsillar GdIgA1 and glomerular GdIgA1 deposition (left, $n = 26$). Oxford classification is shown for each category (right). Correlation data were statistically compared using Spearman's correlation and linear regression analysis. Box plots show median, IQR with whiskers of 1.5 × IQR, and statistically compared using the Mann–Whitney U test (NS; no significance, *$P < 0.05$).

Adaptor-ligation polymerase chain reaction and immunoglobulin sequencing analysis

Total RNA of each dissected tonsillar sample (30 mg) was extracted. Adaptor-ligation polymerase chain reaction (PCR) and immunoglobulin sequencing were performed as previously reported [23]. Briefly, to detect IGHV, IGHD, IGHJ and IGH chain constant (IGHC) gene segment distributions and the deduced complementarity-determining region 3 (CDR3) amino acid sequence of tonsillar IgA, sequence reads were analyzed using bioinformatics software (Repertoire Genesis Incorporation, Ibaraki, Japan) [23, 24]. The reference sequence datasets are available from the International ImMunoGeneTics Information System database (http://www.imgt.org).

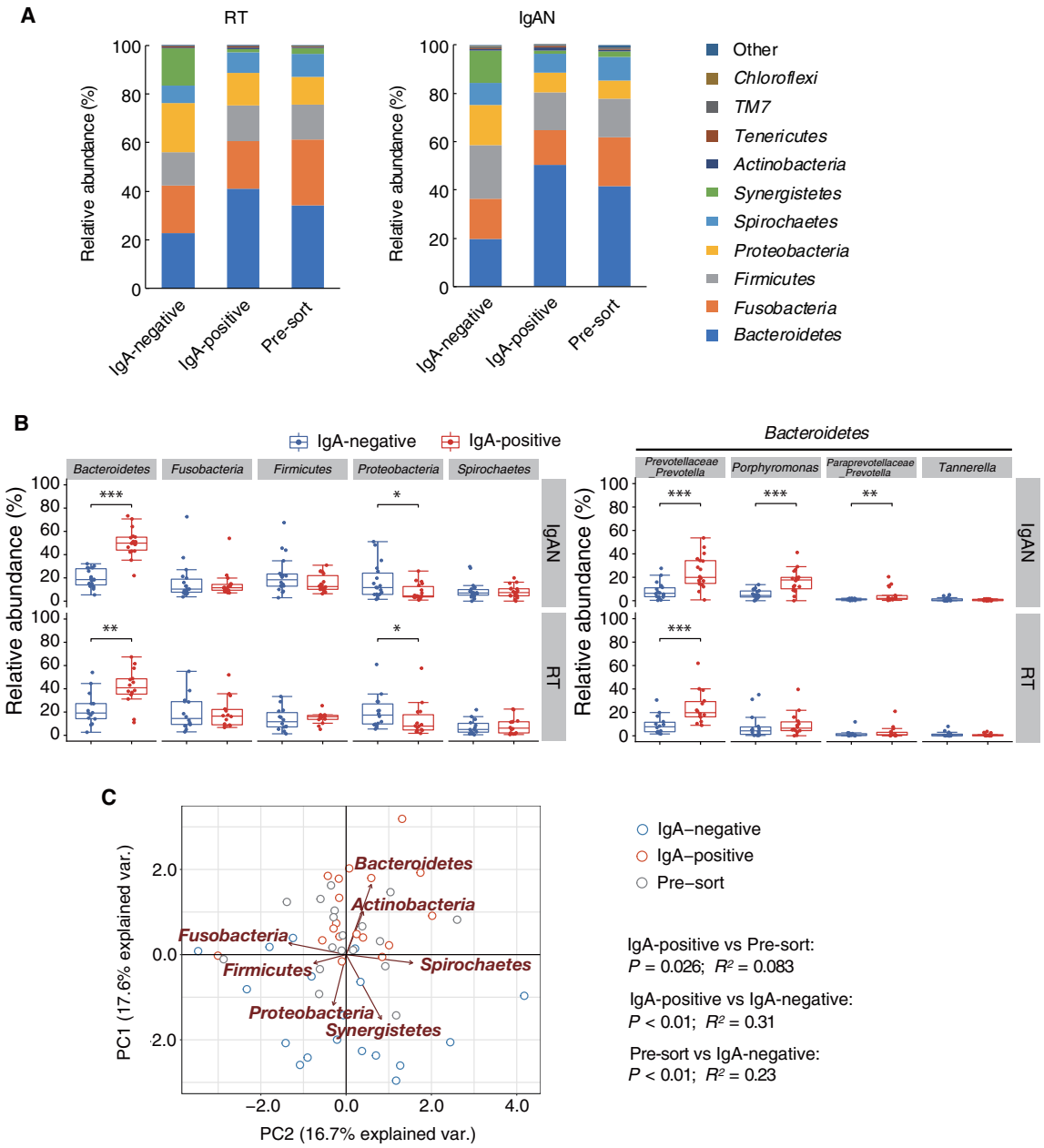

FIGURE 2: IgA-SEQ of tonsillar microbiota. (**A**) The mean relative abundance at the phylum level is shown for the IgA$^+$ and IgA$^-$ fractions and presort samples in the IgAN ($n = 18$) and RT ($n = 14$) groups. (**B**) Relative abundances of the top five phyla (top row) and genera of *Bacteroidetes* (bottom row) are shown for IgA$^+$ (red) and IgA$^-$ (blue) fractions. Data are presented as the median and IQR, and were statistically compared using the Mann–Whitney U test (*P < 0.05, **P < 0.01, ***P < 0.001). (**C**) IgA-SEQ samples of IgAN were clustered using principal coordinate analysis with Bray–Curtis dissimilarities. The length of the black arrows represents taxon abundance. P-values and R^2 values calculated by permutational ANOVA (PERMANOVA) using 9999 permutations based on the Bray–Curtis dissimilarity index are indicated for the IgA$^+$ fraction versus the presort sample, IgA$^+$ versus IgA$^-$ fraction and presort sample versus IgA$^-$ fraction.

Size fractionation

A serum aliquot (200 µL) was fractionated by gel-filtration through a Superdex 200 10/300 column connected to a liquid chromatography system (AKTA Pure 25 L), controlled with Unicorn 7.1 (GE Healthcare, Buckinghamshire, UK). Fractions (500 µL) were collected and analyzed.

Western blotting

Fractionated samples containing 20 ng IgA were subjected to nonreducing 3–8% Tris-acetate gel electrophoresis and electroblotted onto polyvinylidene fluoride membranes. The membranes were blocked, incubated with horseradish peroxidase-conjugated antibodies (Supplementary Methods) and developed using chemiluminescent substrate.

Bacterial culture

Dissected tonsillar tissues were suspended, seeded onto blood-agar plates and anaerobically incubated for 7 days. Following strain detection, *Porphyromonas gingivalis*, *Prevotella intermedia* and *Fusobacterium nucleatum* were cultured in Gifu anaerobic media broth under anaerobic

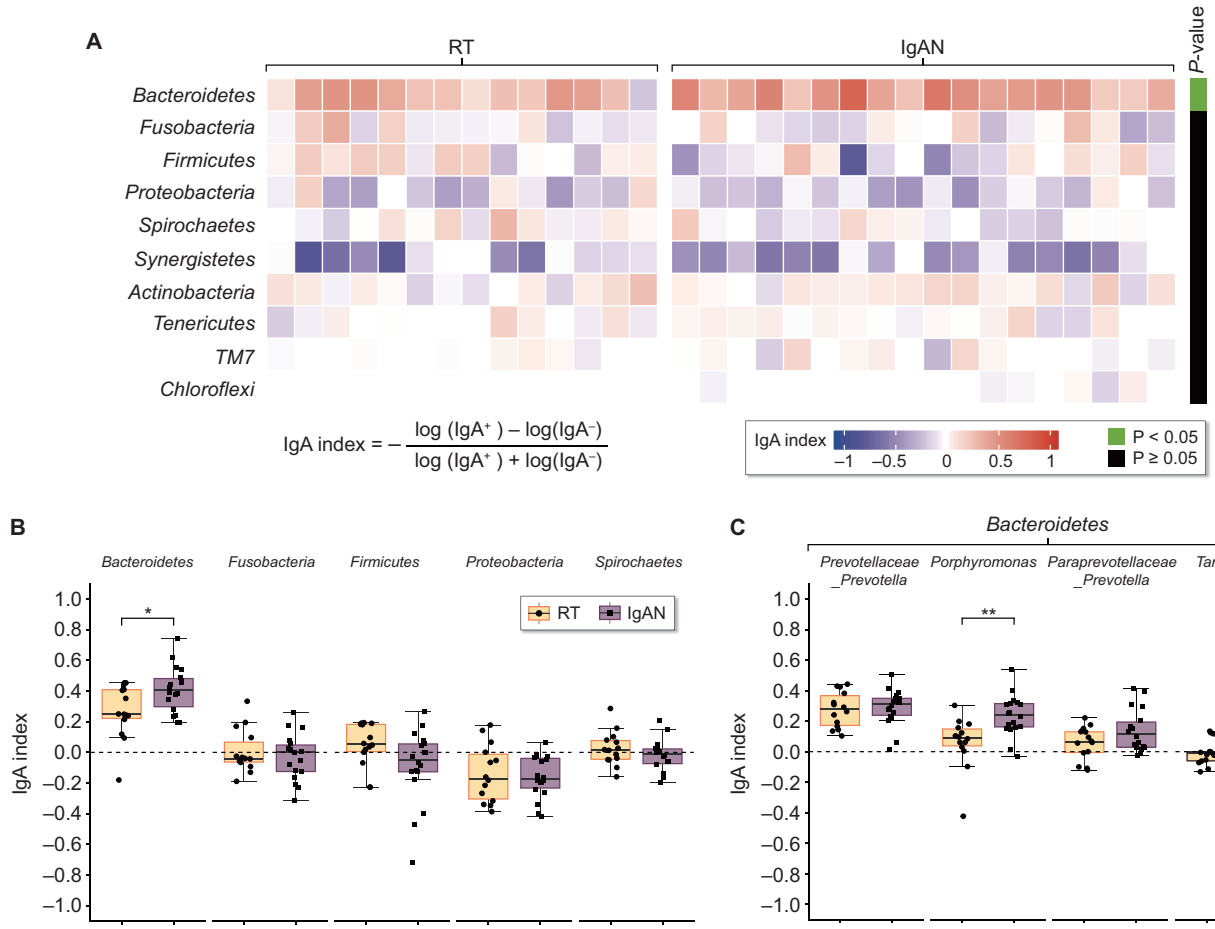

FIGURE 3: IgA index of tonsillar bacteria at the phylum level in IgAN and RT patients. (**A**) Heatmap depicting the IgA index of tonsillar bacterial phyla in IgAN ($n = 18$) and RT patients ($n = 14$). The IgA index ranged from a maximum of +1.0 to a minimum of −1.0; a score near +1.0 indicated that bacteria were more abundant in the IgA^+ fraction. P-values of the IgA index in IgAN patients, as compared with RT patients, are indicated by different colored panels (Mann–Whitney U test, $P < 0.05$; green, $P \geq 0.05$; black). IgA index of tonsillar bacterial phyla (**B**) and top 10 genera (**C**) between the IgAN and RT groups. Box plots show the median and IQR, with whiskers of 1.5 × IQR. Data are presented as the median and IQR (*$P < 0.05$, **$P < 0.01$, Mann–Whitney U test).

conditions. *Escherichia coli* (ATCC 25922) was cultured in Luria–Bertani broth. Isolated bacterial species were assessed by nearly full-length 16S rRNA gene sequencing with 27F/1492R primers [33]. The sequences were compared with the 16S rRNA sequences of each bacterial strain from the DDBJ/EMBL/GenBank database by phylogenetic analysis.

Flow cytometry

IgA binding to bacteria was evaluated using flow cytometry as previously described, with minor modifications [34, 35]. Briefly, after blocking with normal mouse serum, 2.0×10^6 bacteria were incubated with 50 µL of each serum fraction. Sample IgA concentrations were adjusted to that of the F04 fraction prior to incubation. Incubated bacteria were stained with PE-conjugated mouse anti-human IgA monoclonal antibody or mouse IgG1-PE isotype and analyzed using a FACSAria II (Becton Dickinson, Franklin Lakes, NJ, USA).

Statistical analysis

Statistical analyses were performed as described in each figure legend. All statistical data were analyzed using R v. 3.4.2 (https://www.r-project.org). For relative abundance comparisons, the IgA index analysis for each bacterium, and immunoglobulin repertoire sequencing analysis of the IGHV, J and D gene segments and the CDR3 amino acid length, $P < 0.01$ was considered statistically significant. Elsewhere, $P < 0.05$ was accepted. Detailed methods are provided in the Supplementary Methods.

RESULTS

Tonsil and serum APRIL, BAFF and GdIgA1 levels

We enrolled IgAN patients diagnosed by renal biopsy ($n = 62$) and RT patients without urinary abnormalities ($n = 28$) (Table 1). Among these, 48 IgAN and 21 RT cases were included in our previous study [17], and serum samples of 30 IgAN and 7 RT patients prior to tonsillectomy were also available (Supplementary data, Table S1). Tonsillar APRIL and BAFF levels were significantly higher in IgAN than in RT patients ($P = 0.0071$ and $P = 0.025$, respectively), whereas both serum levels were not significantly elevated (Figure 1A and B). Immunohistochemistry in the tonsils using an anti-APRIL monoclonal antibody disclosed diffuse staining in the germinal

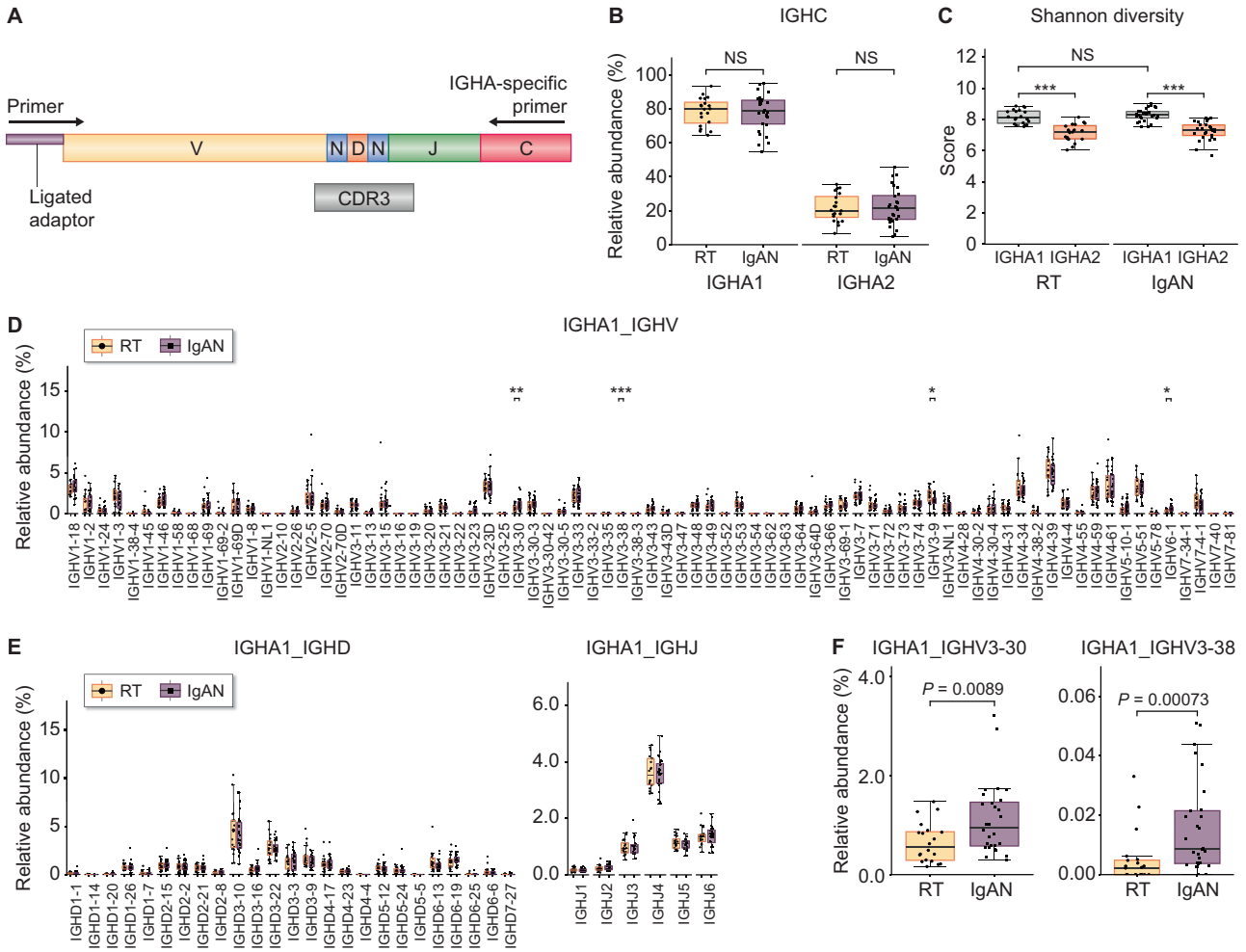

FIGURE 4: Overview of tonsillar IgA heavy chain sequences using AL-PCR. (**A**) Schematic representation of AL-PCR for high-throughput sequencing-based antibody repertoire analysis. A universal primer specific for the IgA heavy chain constant region and an adaptor-primer were used for unbiased IgA gene amplification. Gene amplicons were sequenced using an Illumina MiSeq system, and each sequence read was classified into IgA subclasses by discrimination of the constant region sequence. (**B**) The relative abundance of IGHC (C) gene segments by AL-PCR using the specific primers of the IGHA constant region for the IgAN ($n = 28$) and RT ($n = 20$) groups. (**C**) Shannon diversity scores of IGHA1 and IGHA2 for the IgAN ($n = 28$) and RT ($n = 20$) groups. Relative abundance of IGHV (**D**), IGHD (**E**, left) and IGHJ (**E**, right) with IGHA1 in-frame clones for IgAN ($n = 28$) and RT ($n = 20$) groups. Assigned reads that could not be determined as one clone in each gene segment were excluded from the analysis. Data are presented as median and IQR (NS; no significance, *P < 0.05, **P < 0.01, ***P < 0.001, Mann–Whitney U test). IGHV3-30 and IGHV3-38 differed significantly. (**F**) Relative abundance of IGHA1 with IGHV3-30 (left) and IGHV3-38 (right) in-frame clones for the IgAN ($n = 28$) and RT ($n = 20$) groups are shown (Mann–Whitney U test).

centers, basal cells of the surface epithelium, and perifollicular area around the crypts in both IgAN and RT. A high degree of staining in the germinal centers and perifollicular area was observed in IgAN tonsils with high tonsillar APRIL, whereas epithelial staining was similar across IgAN and RT tonsils (Figure 1C). Depending on the BAFF levels, anti-BAFF antibody mainly labeled the mantle and perifollicular zone of the tonsils in both groups (Figure 1D). Serum but not tonsillar GdIgA1 levels were significantly higher in IgAN than in RT, whereas there was no significant elevation in IgA levels of both serum and tonsils (Figure 1E; Supplementary data, Figure S1A). Tonsillar GdIgA1 levels were significantly correlated with the area of glomerular GdIgA1 deposition and were pathologically associated with mesangial hypercellularity in accordance with the Oxford classification of IgAN (Figure 1F; Supplementary data, Figure S1B). In 16S rRNA gene analysis of IgAN tonsils, relative abundances of phyla including *Bacteroidetes* in patients with higher GdIgA1 levels at the tonsils were significantly different as compared with those with lower GdIgA1 levels when analyzed by permutational multivariate analysis of variance (Supplementary data, Figure S1C and D).

IgA-SEQ of the tonsillar microbiome

We utilized 18 available IgAN tonsillar samples and 14 RT samples for tonsillar microbiota IgA-SEQ analysis. The 16S rRNA gene amplicon sequencing was performed to calculate the relative bacterial abundance in IgA^+ and IgA^- fractions (Supplementary data, Figures S2 and S3A). Taxonomic analysis at the phylum level confirmed that the relative abundance of each phylum in the presort sample was mostly located between the IgA^+ and IgA^- fractions (Figure 2A). At the phylum level, *Bacteroidetes* were significantly more abundant in the IgA^+

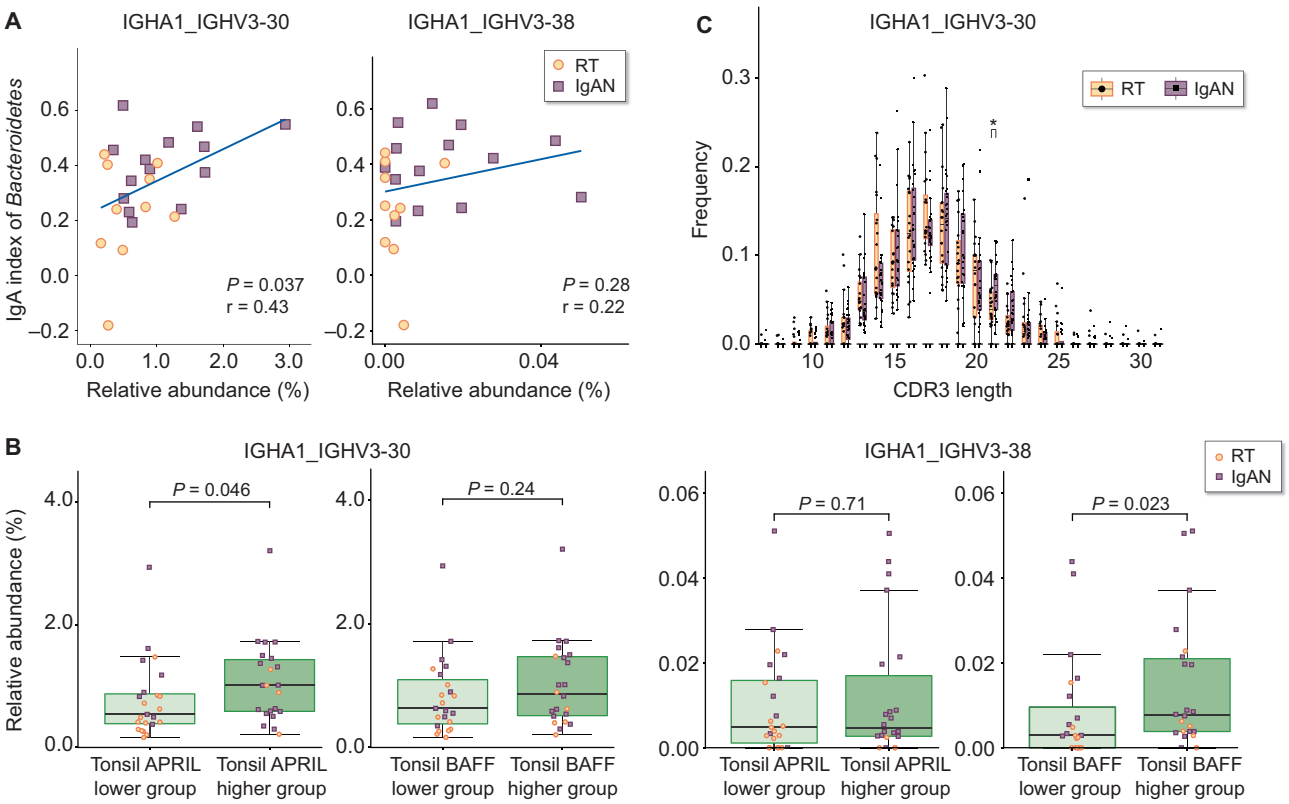

FIGURE 5: Correlations between IGHV3-30/3-38 with IGHA1 clones and the IgA index score of the phylum *Bacteroidetes* and tonsillar APRIL/BAFF levels. (**A**) Correlation between the relative abundance of IGHA1 with IGHV3-30 (left) and IGHV3-38 (right) clones and the IgA index of the phylum *Bacteroidetes* in the IgAN (square) and RT (circle) patient groups, analyzed by both IgA-SEQ and sequencing of the immunoglobulin repertoire ($n = 24$). (**B**) Relative abundance of IGHV3-30 (left) and IGHV3-38 (right) with IGHA1 in patients with tonsillar APRIL (left) and BAFF (right) over the median value was compared with those with APRIL and BAFF values less than the median, respectively. The results of the samples analyzed by both immunoglobulin repertoire sequencing and ELISA of tonsillar APRIL/BAFF ($n = 45$) are shown. (**C**) Frequencies of each CDR3 amino acid length in IGHA1 with IGHV3-30 for the IgAN ($n = 28$) and RT ($n = 20$) groups. Correlation of the data was statistically compared using Pearson's correlation and linear regression analysis. Data are presented as median and IQR (*$P < 0.05$, Mann–Whitney U test). Assigned reads not determined as one clone in each gene segment and out-of-frame reads were excluded from the analysis.

fraction than in the IgA^- fraction (Figure 2B; Supplementary data, Figure S3B) of both groups. At the genus level, relative abundances of *Porphyromonas* and *Prevotella* (phylum *Bacteroidetes*) were significantly higher in the IgA^+ fraction of IgAN. Principal coordinate analysis of the relative bacterial abundances in IgAN showed that each cluster was significantly segregated (Figure 2C). We calculated the IgA index for each bacterium at the phylum and genus levels to identify the tonsillar microbiota selectively coated with IgA in IgAN patients. The IgA index of *Bacteroidetes* was more abundant among bacteria in both IgAN and RT tonsils (Figure 3A). Comparison of the IgA index of each bacterium revealed that the indices of *Bacteroidetes* in IgAN patients were relatively higher ($P = 0.041$) than those in RT patients (Figure 3B). Moreover, the IgA indices of *Porphyromonas* spp. were significantly higher ($P = 0.0015$) in IgAN than in RT (Figure 3C; Supplementary data, Figure S4). These IgA indexes were not associated with clinical (estimated glomerular filtration rate, proteinuria) or pathological findings in IgAN patients (data not shown).

Immunoglobulin repertoire sequencing of tonsillar IgA heavy chain

We designed specific primers for the IgA constant region (Supplementary data, Table S2) to amplify IgA heavy chain-encoding genes [23], and performed adaptor-ligation PCR and immunoglobulin repertoire sequencing using tonsillar RNA samples from 28 IgAN and 20 RT patients (Figure 4A; Supplementary data, Table S3). The relative abundance of IGHC clones in each sample showed that ~80% was assigned to IGHA1 (Figure 4B). Diversity index analysis of immunoglobulin clones revealed significantly higher Shannon diversity scores for IGHA1 than IGHA2 (Figure 4C). Comparison of the relative abundance of IGHV, IGHD and IGHJ segments with IGHA1 clones revealed significantly higher IGH variable 3-30 (IGHV3-30) ($P = 0.0089$) and IGHV3-38 ($P = 0.00073$) expression in IgAN than that in RT tonsils (Figure 4D and F). IGHJ and IGHD segments exhibited no significant difference (Figure 4E).

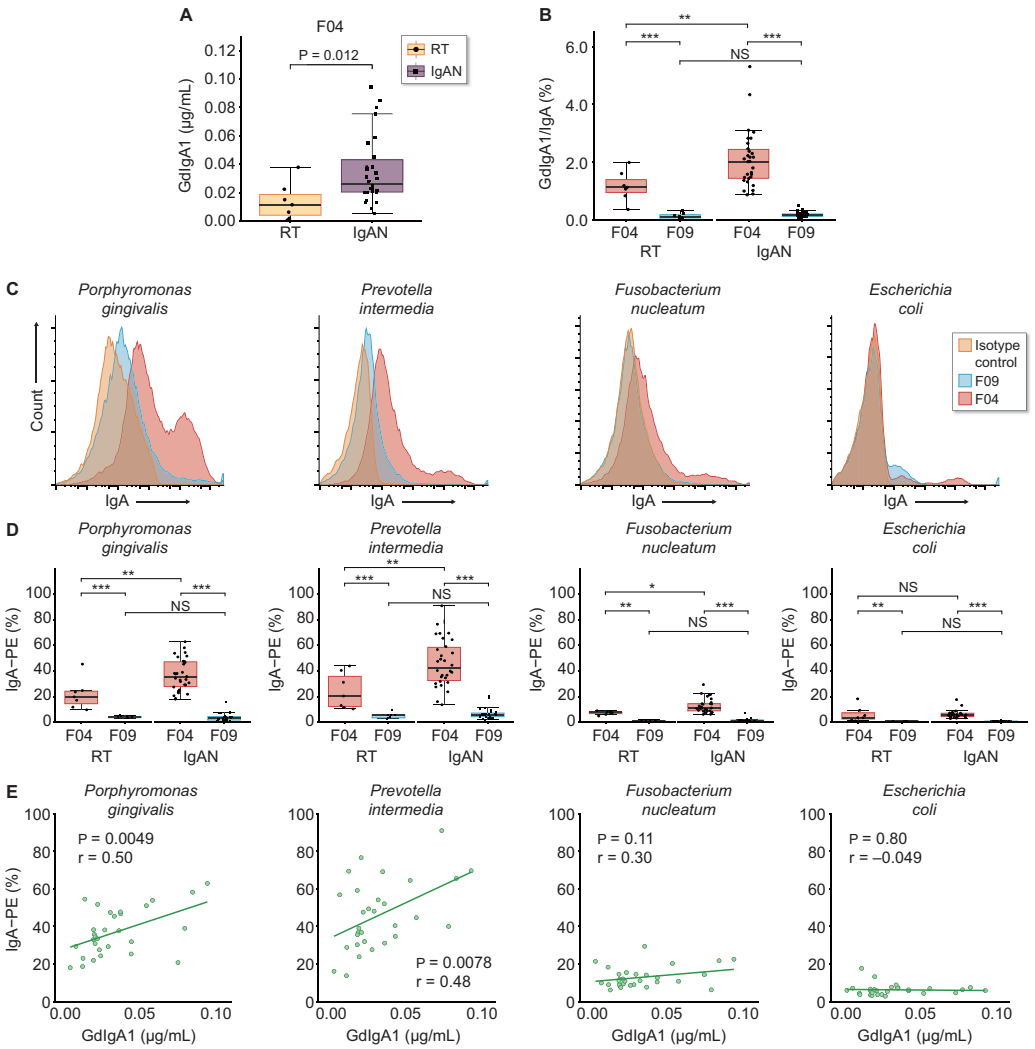

FIGURE 6: Analysis of the binding abilities of IgA complexes to cultured bacteria by flow cytometry. (**A**, **B**) GdIgA1 levels in the F04 fraction and (A) GdIgA1/IgA ratio in the F04 and F09 fraction (B) from IgAN ($n = 30$) and RT ($n = 7$) patients. Box plots show the median and IQR, with whiskers of 1.5 × IQR. Data were statistically compared using the Mann–Whitney U test (NS; no significance, $^{**}P < 0.01$, $^{***}P < 0.001$). (**C**) The serum mIgA (F09) and pIgA (F04) fractions were examined for the ability of IgA to bind the surface of cultured bacteria by flow cytometry using an anti-IgA monoclonal antibody. *Porphyromonas gingivalis*, *Prevotella intermedia* and *Fusobacterium nucleatum* were isolated and cultured from dissected tonsils of IgAN patients, whereas *Eschericia coli* was obtained as an ATCC standard strain. Each histogram represents the intensity of IgA binding by isotype-control (yellow), F09 (blue) and F04 (red) fractions. The concentrations of IgA of F09 fractions were adjusted to that of the F04 fraction in each sample. (**D**) Percent positivity for IgA-PE over the isotype-control for each bacterial cell by F09 and F04 fractions in patients with IgAN ($n = 30$) and RT ($n = 7$). Box plots show the median and IQR, with whiskers of 1.5 × IQR. Data were statistically compared using the Mann–Whitney U test (NS; no significance, $^{*}P < 0.05$, $^{**}P < 0.01$, $^{***}P < 0.001$). (**E**) Correlation between the percent positivity for IgA-PE for each bacterial species and the levels of GdIgA1 by F04 fractions in patients with IgAN ($n = 30$). Data were statistically compared using Pearson's correlation and linear regression analysis.

Correlation of IgA1 expression with IGHV3-30 clones to *Bacteroidetes* IgA index score and tonsillar APRIL expression

In IGHV3-30 clones, the IgA index of the phylum *Bacteroidetes* was significantly ($P = 0.0089$) and positively correlated with only the relative abundance of IGHA1, whereas IGHV3-38 clones showed no significant correlation (Figure 5A). Further, the relative abundance of IGHJ3 recombining with IGHV3-30 of IGHA1 clones was significantly higher ($P = 0.0073$) in IgAN tonsils and was positively correlated ($P = 0.030$) with the *Bacteroidetes* IgA index (Supplementary data, Figure S5 and Table S4). Moreover, the relative abundance of IGHA1 with IGHV3-30 clones was significantly higher ($P = 0.046$) in patients with high- rather than low-tonsillar APRIL levels, but not tonsillar BAFF levels. However, the relative abundance of IGHA1 with IGHV3-38 clones was significantly higher ($P = 0.023$) in patients with high- rather than low-tonsillar BAFF levels, but not tonsillar APRIL levels (Figure 5B). CDR3 amino acid length distribution in IGHA1 with IGHV3-30 displayed similar Gaussian distribution in IgAN and RT patients (Figure 5C).

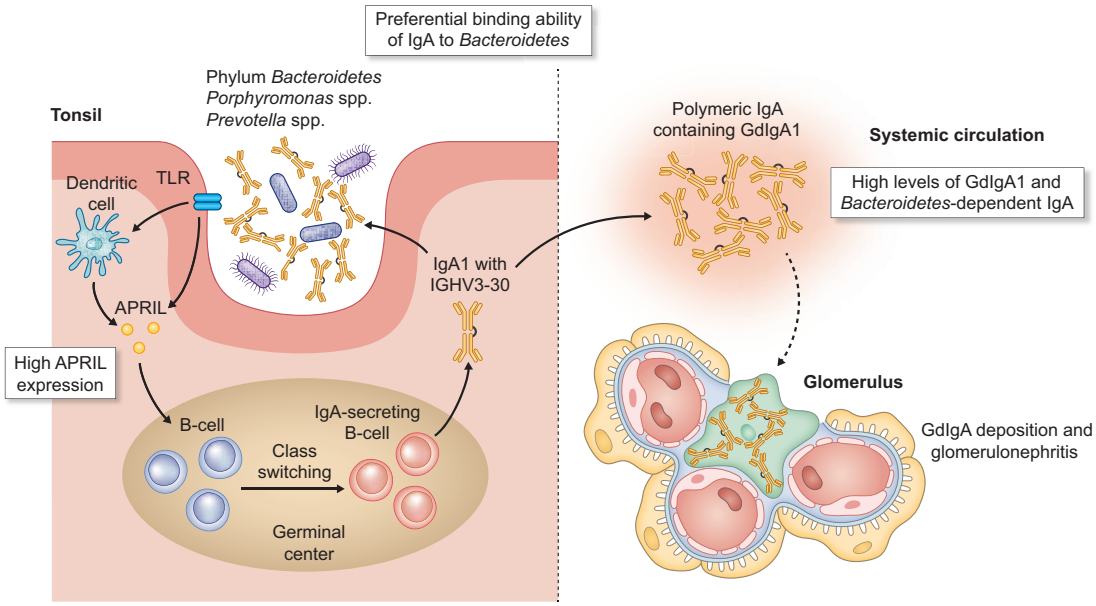

FIGURE 7: Overview of aberrant mucosal immunoreaction in IgAN patients. This study indicated that the aberrant immunoreaction at tonsillar crypts and corresponding *Bacteroidetes* bacteria dependent polymeric IgA, are involved in IgAN pathogenesis. Enclosed documents indicate the characteristic findings in IgAN patients.

Flow cytometry-based analysis of IgA binding to tonsillar bacteria

Serum fractionation was performed using high-performance liquid chromatography with a gel-filtration column, as previously reported [36] (Supplementary data, Figure S6A and B). The F04 (∼650 kDa) containing the immunoglobulin J-chain (Supplementary data, Figure S6C) and F09 (∼150 kDa) fractions were selected as serum pIgA- and mIgA-containing fractions from IgAN and RT tonsils. The pIgA fraction levels of GdIgA1 ($P = 0.012$) and GdIgA1/IgA ratios ($P = 0.0092$) were significantly higher in IgAN than in RT (Figure 6A and B), whereas IgA levels were comparable (Supplementary data, Figure S6D). IgA–IgG complex in pIgA fraction was also significantly higher in IgAN than in RT (Supplementary data, Figure S6E). Following IgA concentration adjustment, F04 and F09 fractions were incubated with each bacterium to evaluate IgA binding (Supplementary data, Figure S7). Flow cytometry (Figure 6C; Supplementary data, Figure S8A) revealed that F04 fractions yielded significantly higher proportions of IgA^+ bacteria for each bacterium than F09 fractions (Figure 6D). Similarly, IgA in the IgAN F04 fractions exhibited high-binding activities with each bacterium, particularly *Porphyromonas gingivalis*, compared with RT fractions. IgA binding intensity toward *Porphyromonas gingivalis* and *Prevotella intermedia* significantly correlated with both GdIgA1 and IgA–IgG serum levels in IgAN F04 fractions (Figure 6E; Supplementary data, Figure S8B).

DISCUSSION

In this study, we showed that in IgAN patients, members of the phylum *Bacteroidetes*, especially *Porphyromonas* spp., were more frequently coated with IgA in the tonsils. Further, these could be bound with serum pIgA having higher GdIgA1 levels compared with those in RT tonsils. Moreover, immunoglobulin repertoire analysis using tonsillar IgA revealed higher IGHV3-30 expression with IGHA1 clones in IgAN patients than in RT patients, significantly correlating with the *Bacteroidetes* IgA index (Figure 7). Our findings suggested that perturbed immunity against a distinct tonsillar microbiota subset may be important in IgAN pathogenesis.

We applied IgA-SEQ to the tonsillar microbiome to determine immunogenic microbiota related to IgAN pathophysiology. *Bacteroidetes* were markedly coated with IgA in the tonsillar crypts. IgA-coated *Porphyromonas* spp. exhibited a significantly higher enrichment score in IgAN than RT tonsils. Moreover, tonsillar APRIL and BAFF levels, both important for the reaction of mucosal IgA to microbiota [15] via T-cell-independent pathways [13, 14], were significantly higher in IgAN than in RT tonsils. These data suggested that IgA antibodies are polyreactive to some microbiota, such as members of *Bacteroidetes* (especially *Porphyromonas* spp.) and may be preferentially produced in IgAN tonsils. However, antigen-specific IgA may also be produced via T-cell-dependent pathways at these sites.

To examine the mechanism for IgA binding to the microbiota, we conducted high-throughput sequencing of the tonsillar IgA repertoire. A higher amount of IGHV3-30 in IgA was observed in IgAN patient tonsils. Significant correlation with the degree of *Bacteroidetes* coated with IgA suggests the involvement of the IGHV3-30 of IgA in IgA binding with *Bacteroidetes*. Furthermore, a significant association between tonsillar APRIL levels and IGHA1 expression with IGHV3-30 clones implied that the T-cell-independent pathway may

be involved in IgA prevalence, with IGHV3-30 being polyreactive to a subset of microbiota. IgA produced via the T-cell-independent pathway is more polyreactive with microbiota than T-cell-dependent pathway-associated IgA [37]. In this study, Gaussian distributions of the length of CDR3 in both groups indicated little distinct clonal expansion under the particular antigenic pressure in IgAN patients. Additionally, tonsillar BAFF in IgAN patients was significantly associated with IGHV3-38, another repertoire significantly elevated in IgAN. BAFF acts on B-cell survival and maturation, and in concert with APRIL for class switching to IgA via shared receptors [38]. This may therefore reflect divergent effects of these tumor necrosis factor (TNF) superfamily molecules. Compared with IGHV3-38, the abundance of which was low among the IgA1 repertoire, consistency of association between IGHV3-30, APRIL and IgA response to microbiota may be weighted by APRIL of the genome-wide association study risk loci for IgAN [4, 39].

Consistent with the IgA-SEQ data, *Bacteroidetes* bacteria were coated with the serum pIgA fraction to a greater extent in IgAN patients than in RT patients. These findings supported the hypothesis that mucosa-derived IgA is increased in IgAN patient serum. BAFF-transgenic mice [34] exhibited increased serum commensal-dependent polymeric GdIgA, indicating the similarities between human and murine IgAN. GdIgA1 levels in the polymeric fraction were significantly increased and were highly correlated with IgA binding with *Bacteroidetes* in IgAN. This suggests that mucosal GdIgA1 in the tonsils of IgAN patients was mistakenly transported to other sites via BAFF and APRIL. As IgA harboring J-chain is exclusively detected in the polymeric fraction, IgA with IGHV3-30 or 3-38 repertoire could be present in the polymeric form of IgA if dimeric IgA is translocated from the mucosa. Whether these repertoires are involved in polymeric and immune-complex formation remains unclear.

The role of microbiota-dependent IgA in IgAN development is not fully elucidated. However, in the above IgAN models, commensal-dependent IgA was detected in the glomeruli [34]. Conversely, mucosal microbiota depletion by antibiotic administration reduced IgA deposition in humanized murine glomeruli, accompanied with reduced levels of IgA–IgG complexes [40]. Our study also indicated significant associations between tonsillar GdIgA1 levels and glomerular GdIgA1 deposition and mesangial hypercellularity, and between pIgA binding to *Bacteroidetes* and IgA–IgG complexes. No differences were noted in the tonsillar GdIgA1 levels between IgAN and RT. However, tonsillar GdIgA1 may have different repertoire diversity between both groups, much like IgA1. Discrimination of tonsillar GdIgA1 levels by tonsillar microbiome abundance could substantiate this. Collectively, these data strongly suggested that microbiota-dependent IgA, which was significantly increased in the serum of IgAN patients, underlies glomerular immune-complex deposition and is thus involved in IgAN pathogenesis.

We acknowledged several limitations in this study. First, we collected palatine tonsils from RT patients as control samples because tonsillar samples from healthy subjects were unavailable. However, gram-negative anaerobic bacteria are potentially associated with tonsillitis [41], suggesting that the RT tonsillar microbiome may contain more abundant anaerobic bacteria than that from healthy subjects. Second, not all serum and tonsillar crypt samples were available for IgA-SEQ, IgA repertoire and bacterial FACS analyses, potentially causing some selective bias and lack of power for detecting real differences. However, despite limited samples, we detected statistically robust differences in serum GdIgA1 levels between IgAN and RT, consistent with previous reports [42–44]. Further, our results were consistent across the study. We, therefore, surmised that adequate analyses could be conducted to provide meaningful findings. Lastly, most patients were enrolled in the early stage of IgAN, which affects the correlation between IgA immune response and clinical findings. Future studies with larger samples will, therefore, be needed.

In conclusion, this study provides evidence that tonsillar immune responses, particularly against *Bacteroidetes*, were perturbed in IgAN patients. These data provided crucial insights into aberrant mucosal immunoreactions against the host tonsillar microbiome and indicate potentially novel therapeutic targets for IgAN management.

SUPPLEMENTARY DATA

Supplementary data are available at ndt online.

ACKNOWLEDGEMENTS

The authors acknowledge the technical assistance of Naofumi Imai, Kaori Takahashi, Fumiko Kusama, Akiko Seino and Tomoko Ubara. The authors also thank Dr Daisuke Kondo from the Department of Nephrology and Rheumatology at Niigata City General Hospital, Dr Hajime Yamazaki from the Department of Internal Medicine at Nagaoka Red Cross Hospital, Dr Ryuji Aoyagi from the Department of Nephrology at Tachikawa General Hospital and Dr Takuma Takata from the Department of Nephrology at Nagaoka Chuo General Hospital for contributing to sample collection. Preliminary data from this study were presented in a poster session at the American Society of Nephrology Kidney Week 2018, San Diego, Kidney Week 2019, Washington, DC, USA and in an English oral session at the 61st Annual Meeting of the Japanese Society of Nephrology, Niigata, Japan, in 2018.

FUNDING

This study was supported by a Grant-in-Aid for Scientific Research (B) (no. 19H03674 to I.N.); a Grant-in-Aid for Scientific Research (C) (no. 18K08234 to S.G.) from the Ministry of Education, Culture, Sports, Science and Technology of Japan; and a Grant-in-Aid for Scientific Research on Innovative Areas “Genome Science” from the Ministry of Education, Culture, Sports, Science and Technology of Japan (221S0002).

AUTHORS' CONTRIBUTIONS

S.G. and I.N. designed the study; H.Y. carried out the experiments, analyzed the data and generated the figures; N.T. performed surgical procedures; H.Y., M.T. and H.W. collected samples; H.Y., K.H., H.M., Y.N. and K.K. analyzed the sequencing data; H.Y., S.G., S.Y., Y.K., A.H. and I.N. drafted and revised the article; all authors approved the final version of the manuscript.

CONFLICT OF INTEREST STATEMENT

None declared.

REFERENCES

1. Wyatt RJ, Julian BA. IgA nephropathy. *N Engl J Med* 2013; 368: 2402–2414
2. Hotta O, Miyazaki M, Furuta T *et al.* Tonsillectomy and steroid pulse therapy significantly impact on clinical remission in patients with IgA nephropathy. *Am J Kidney Dis* 2001; 38: 736–743
3. Hirano K, Matsuzaki K, Yasuda T *et al.* Association between tonsillectomy and outcomes in patients with immunoglobulin A nephropathy. *JAMA Netw Open* 2019; 2: e194772–11
4. Kiryluk K, Li Y, Scolari F *et al.* Discovery of new risk loci for IgA nephropathy implicates genes involved in immunity against intestinal pathogens. *Nat Genet* 2014; 46: 1187–1196
5. Kiryluk K, Novak J. The genetics and immunobiology of IgA nephropathy. *J Clin Invest* 2014; 124: 2325–2332
6. Novak J, Vu HL, Novak L *et al.* Interactions of human mesangial cells with IgA and IgA-containing immune complexes. *Kidney Int* 2002; 62: 465–475
7. Suzuki H, Kiryluk K, Novak J *et al.* The pathophysiology of IgA nephropathy. *J Am Soc Nephrol* 2011; 22: 1795–1803
8. Oruc Z, Oblet C, Boumediene A *et al.* IgA structure variations associate with immune stimulations and IgA mesangial deposition. *J Am Soc Nephrol* 2016; 27: 2748–2761
9. Brandtzaeg P. Presence of J chain in human immunocytes containing various immunoglobulin classes. *Nature* 1974; 252: 418–420
10. Hemmi H, Takeuchi O, Kawai T *et al.* A Toll-like receptor recognizes bacterial DNA. *Nature* 2000; 408: 740–745
11. Suzuki H, Suzuki Y, Narita I *et al.* Toll-like receptor 9 affects severity of IgA nephropathy. *J Am Soc Nephrol* 2008; 19: 2384–2395
12. Tezuka H, Abe Y, Asano J *et al.* Prominent role for plasmacytoid dendritic cells in mucosal T cell-independent IgA induction. *Immunity* 2011; 34: 247–257
13. Litinskiy MB, Nardelli B, Hilbert DM *et al.* DCs induce CD40-independent immunoglobulin class switching through BLyS and APRIL. *Nat Immunol* 2002; 3: 822–829
14. He B, Xu W, Santini PA *et al.* Intestinal bacteria trigger T cell-independent immunoglobulin A(2) class switching by inducing epithelial-cell secretion of the cytokine APRIL. *Immunity* 2007; 26: 812–826
15. Fagarasan S, Kawamoto S, Kanagawa O *et al.* Adaptive immune regulation in the gut: T cell–dependent and T cell–independent IgA synthesis. *Annu Rev Immunol* 2010; 28: 243–273
16. Muto M, Manfroi B, Suzuki H *et al.* Toll-like receptor 9 stimulation induces aberrant expression of a proliferation-inducing ligand by tonsillar germinal center B cells in IgA nephropathy. *J Am Soc Nephrol* 2017; 28: 1227–1238
17. Watanabe H, Goto S, Mori H *et al.* Comprehensive microbiome analysis of tonsillar crypts in IgA nephropathy. *Nephrol Dial Transplant* 2017; 32: 2072–2079
18. Bunker JJ, Flynn TM, Koval JC *et al.* Innate and adaptive humoral responses coat distinct commensal bacteria with immunoglobulin A. *Immunity* 2015; 43: 541–553
19. Roche AM, Richard AL, Rahkola JT *et al.* Antibody blocks acquisition of bacterial colonization through agglutination. *Mucosal Immunol* 2015; 8: 176–185
20. Honda K, Littman DR. The microbiota in adaptive immune homeostasis and disease. *Nature* 2016; 535: 75–84
21. Palm NW, de Zoete MR, Cullen TW *et al.* Immunoglobulin A coating identifies colitogenic bacteria in inflammatory bowel disease. *Cell* 2014; 158: 1000–1010
22. Viladomiu M, Kivolowitz C, Abdulhamid A *et al.* IgA-coated *E. coli* enriched in Crohn's disease spondyloarthritis promote T_H17-dependent inflammation. *Sci Transl Med* 2017; 9: eaaf9655
23. Kitaura K, Yamashita H, Ayabe H *et al.* Different somatic hypermutation levels among antibody subclasses disclosed by a new next-generation sequencing-based antibody repertoire analysis. *Front Immunol* 2017; 8: 389
24. Ichinohe T, Miyama T, Kawase T *et al.* Next-generation immune repertoire sequencing as a clue to elucidate the landscape of immune modulation by host–gut microbiome interactions. *Front Immunol* 2018; 9: 668
25. Schatz DG, Swanson PC. V(D)J recombination: mechanisms of initiation. *Annu Rev Genet* 2011; 45: 167–202
26. Muramatsu M, Kinoshita K, Fagarasan S *et al.* Class switch recombination and hypermutation require activation-induced cytidine deaminase (AID), a potential RNA editing enzyme. *Cell* 2000; 102: 553–563
27. Chen Y, Chaudhary N, Yang N *et al.* Microbial symbionts regulate the primary Ig repertoire. *J Exp Med* 2018; 215: 1397–1415
28. Matousovic K, Novak J, Yanagihara T *et al.* IgA-containing immune complexes in the urine of IgA nephropathy patients. *Nephrol Dial Transplant* 2006; 21: 2 478–2484
29. Yasutake J, Suzuki Y, Suzuki H *et al.* Novel lectin-independent approach to detect galactose-deficient IgA1 in IgA nephropathy. *Nephrol Dial Transplant* 2015; 30: 1315–1321
30. Prasad K, Prabhu GK. Image analysis tools for evaluation of microscopic views of immunohistochemically stained specimen in medical research–a review. *J Med Syst* 2012; 36: 2621–2631
31. Jensen EC. Quantitative analysis of histological staining and fluorescence using ImageJ. *Anat Rec* 2013; 296: 378–381
32. Kau AL, Planer JD, Liu J *et al.* Functional characterization of IgA-targeted bacterial taxa from undernourished Malawian children that produce diet-dependent enteropathy. *Sci Transl Med* 2015; 7: 276ra24
33. Weisburg WG, Barns SM, Pelletier DA *et al.* 16S ribosomal DNA amplification for phylogenetic study. *J Bacteriol* 1991; 173: 697–703
34. McCarthy DD, Kujawa J, Wilson C *et al.* Mice overexpressing BAFF develop a commensal flora–dependent, IgA-associated nephropathy. *J Clin Invest* 2011; 121: 3991–4002
35. Slack E, Hapfelmeier S, Stecher B *et al.* Innate and adaptive immunity cooperate flexibly to maintain host-microbiota mutualism. *Science* 2009; 325: 617–620
36. Moura IC, Arcos-Fajardo M, Sadaka C *et al.* Glycosylation and size of IgA1 are essential for interaction with mesangial transferrin receptor in IgA nephropathy. *J Am Soc Nephrol* 2004; 15: 622–634
37. Berkowska MA, Schickel J-N, Grosserichter-Wagener C *et al.* Circulating human CD27-IgA+ memory B cells recognize bacteria with polyreactive Igs. *J Immunol* 2015; 195: 1417–1426
38. Vincent FB, Morand EF, Schneider P *et al.* The BAFF/APRIL system in SLE pathogenesis. *Nat Rev Rheumatol* 2014; 10: 365–373
39. Yu XQ, Li M, Zhang H *et al.* A genome-wide association study in Han Chinese identifies multiple susceptibility loci for IgA nephropathy. *Nat Genet* 2012; 44: 178–182
40. Chemouny JM, Gleeson PJ, Abbad L *et al.* Modulation of the microbiota by oral antibiotics treats immunoglobulin A nephropathy in humanized mice. *Nephrol Dial Transplant* 2019; 34: 1135–1144
41. Brook I. The role of anaerobic bacteria in tonsillitis. *Int J Pediatr Otorhinolaryngol* 2005; 69: 9–19
42. Hiki Y, Odani H, Takahashi M *et al.* Mass spectrometry proves under-O-glycosylation of glomerular IgA1 in IgA nephropathy. *Kidney Int* 2001; 59: 1077–1085
43. Moldoveanu Z, Wyatt RJ, Lee JY *et al.* Patients with IgA nephropathy have increased serum galactose-deficient IgA1 levels. *Kidney Int* 2007; 71: 1148–1154
44. Gharavi AG, Moldoveanu Z, Wyatt RJ *et al.* Aberrant IgA1 glycosylation is inherited in familial and sporadic IgA nephropathy. *J Am Soc Nephrol* 2008; 19: 1008–1014

Received: 22.1.2020; Editorial decision: 7.7.2020

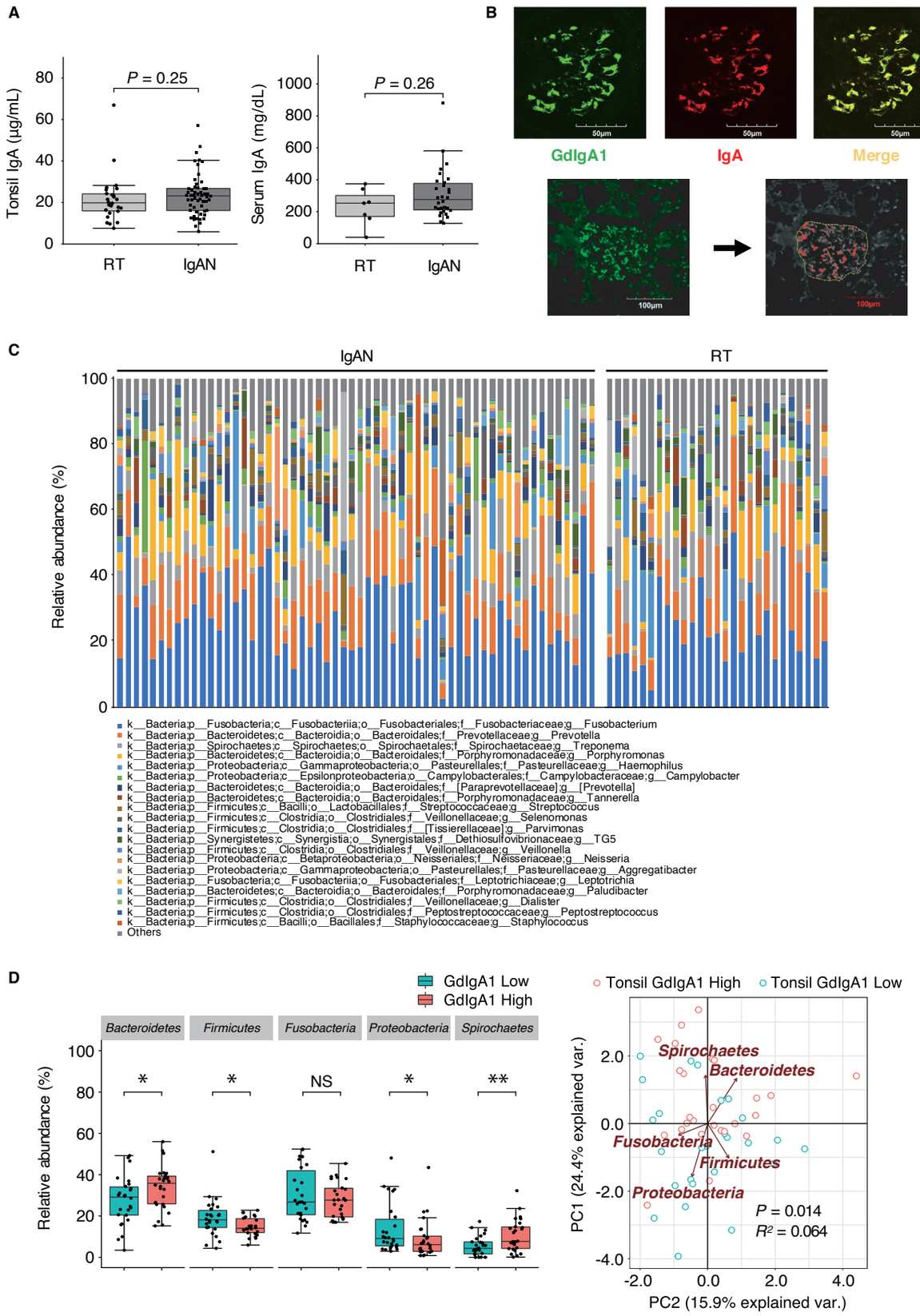

FIGURE S1: Association between GdIgA1 expression and bacterial composition in tonsillar crypts. (**A**) Levels of IgA of adjusted tonsillar protein solution from IgAN (n = 55) and RT (n = 26) (left) patients and serum from IgAN (n = 30) and RT (n = 7) (right) patients. (**B**) Overview of the evaluation of glomerular area immunostaining with anti-GdIgA1 monoclonal antibody. Immunohistochemical staining with anti-GdIgA1 monoclonal antibody (KM55) was performed on paraffin-embedded sections of renal biopsy specimens from IgAN patients. GdIgA1 is mainly localized in the mesangial area with IgA (top, Scale bars; 50 μm.). FITC positively stained area was quantified using ImageJ software to calculate the proportion of positively stained area per glomerulus (bottom). (**C**) Relative abundances of tonsillar bacteria at the genus level are shown for IgAN (n = 58) and RT (n = 27). Stacked bar charts indicate the top 20 genera. (**D**) Relative abundances of the top five tonsillar bacteria at the phylum level in IgAN patients exhibiting both high tonsillar GdIgA1 (n = 26) and low tonsillar GdIgA1 (n = 26) are shown (left). Total bacterial compositions in tonsils of IgAN patients were clustered using principal coordinate analysis (right) with Bray–Curtis dissimilarities between the group of high (green) and low (red) tonsillar GdIgA1 levels. *P*-values and R squared values calculated by PERMANOVA using 9,999 permutations based on the Bray–Curtis dissimilarity index are indicated. The length of brown arrows represents taxa abundance.

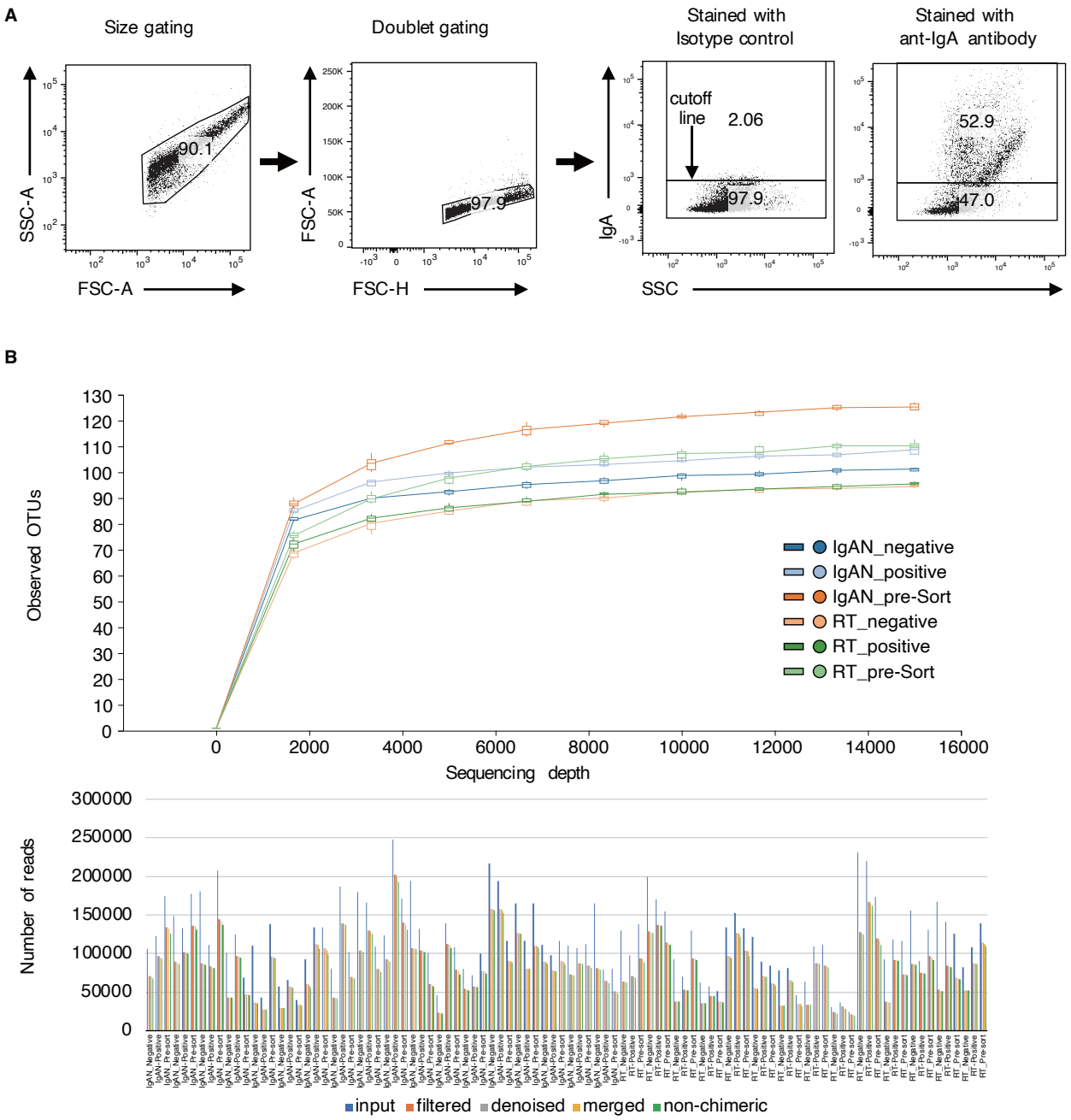

FIGURE S2: Gating strategy of flow cytometry, rarefaction analysis, and the number of each read for tonsillar IgA-SEQ. (**A**) Gating strategy for tonsillar IgA-SEQ samples. The population was first gated using SSC-A and FSC-A, and doublet cells were removed before analyzing the fluorescence signal. Samples stained with isotype-control antibody were used to determine the fluorescence intensity corresponding to unspecific binding, before being used as a pre-sort sample for 16S rRNA gene amplicon sequencing. Fluorescence intensities greater than the threshold of the isotype-control–stained sample were considered to indicate IgA-positive bacteria. (**B**) Rarefaction plots (top) and the number of obtained reads (bottom) in IgA-positive and IgA-negative fractions and the pre-sort samples of IgAN (n = 18) and RT (n = 14). The cutoff point was considered to be 8,000 reads per sample. We obtained > 19, 485 and an average of 80,391 features per sample in tonsillar IgA-SEQ analysis.

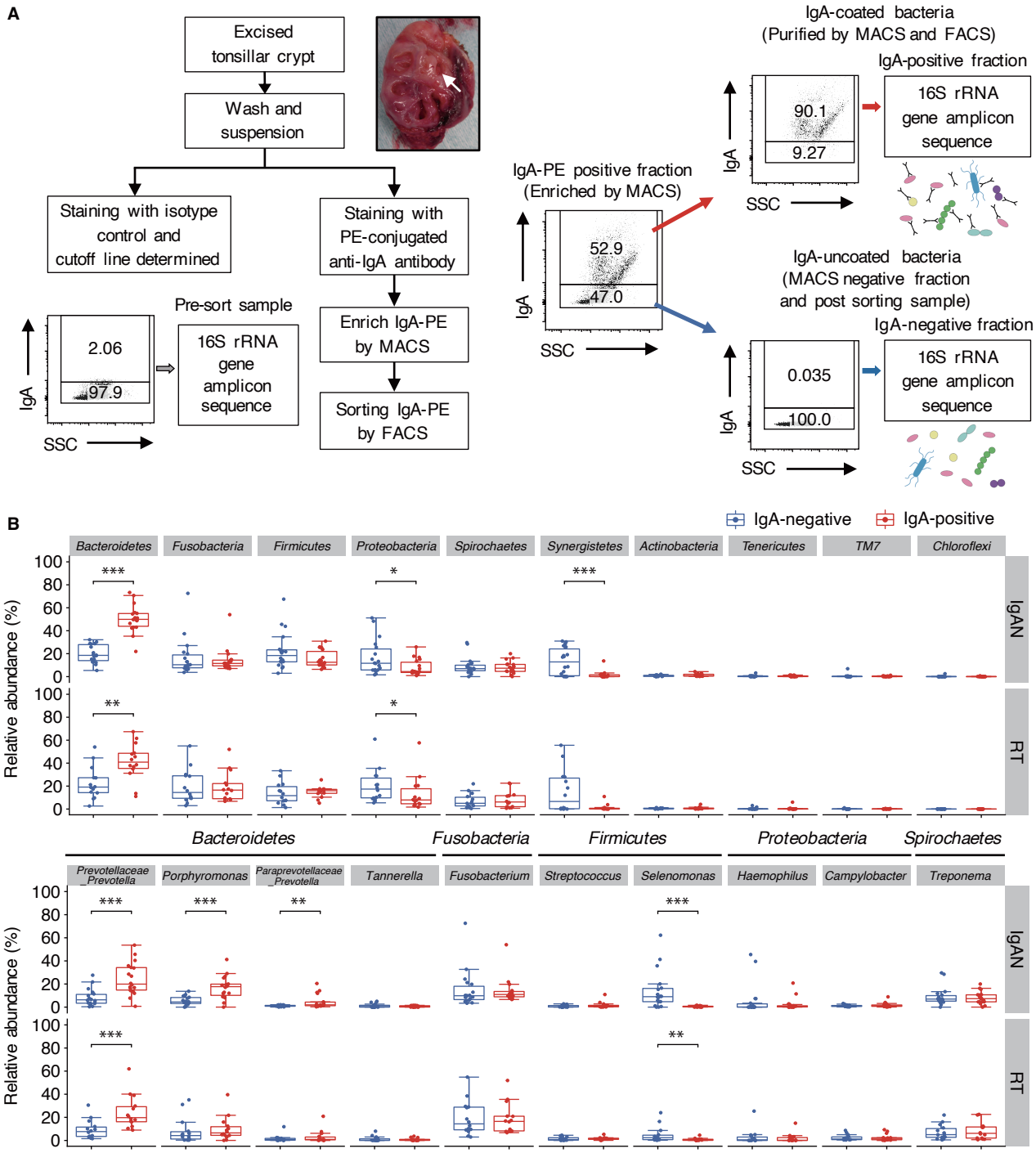

FIGURE S3: Detailed data for IgA-SEQ of tonsillar microbiota. (**A**) Workflow of IgA-based sorting of tonsillar bacteria combined with sequencing of the 16S rRNA gene amplicon (IgA-SEQ). Excised tonsillar crypts (white arrow) were washed and suspended. Supernatants of tonsillar samples were centrifuged and collected as bacterial pellets. After blocking, suspended pellets were divided into two samples: stained with PE-conjugated mouse anti-human IgA antibodies as IgA-PE-stained samples and mouse IgG1-PE isotype as the pre-sort sample for flow cytometric analysis. Pre-sort samples were used to determine the cutoff line of PE fluorescence intensity by FACS. IgA-PE-stained bacterial samples were enriched with MACS and sorted by FACS into IgA-positive and IgA-negative fractions. The MACS-negative fraction was added to the post-sorted IgA-negative fraction, and was considered indicative of a true IgA-negative fraction. Genomic DNA from each fraction was extracted and subjected to 16S rRNA gene amplicon sequencing. (**B**) Relative abundance of tonsillar bacterial top 10 phyla (top) and genera (bottom) between the IgAN and RT groups. Box plots show the median and IQR, with whiskers of 1.5 × IQR. Data are presented as the median and IQR (*$P < 0.05$, **$P < 0.01$, Mann–Whitney U test).

FIGURE S4: IgA index of tonsillar bacteria at the genus level in IgAN and RT patients. Heatmap depicting the IgA index of tonsillar bacterial genera in IgAN (n = 18) and RT (n = 14) patients. Heatmap only depicts bacterial genera with relative abundance > 0.001 in the pre-sort sample from the analysis. The color panel on the right side indicates the IgA indices that were higher in patients with IgAN compared with RT (Mann–Whitney U test; $P < 0.01$, pink; $P < 0.05$. green; $P \geq 0.05$, black). Purple color indicates IgA indices that were higher in RT patients compared with those with IgAN ($P < 0.05$).

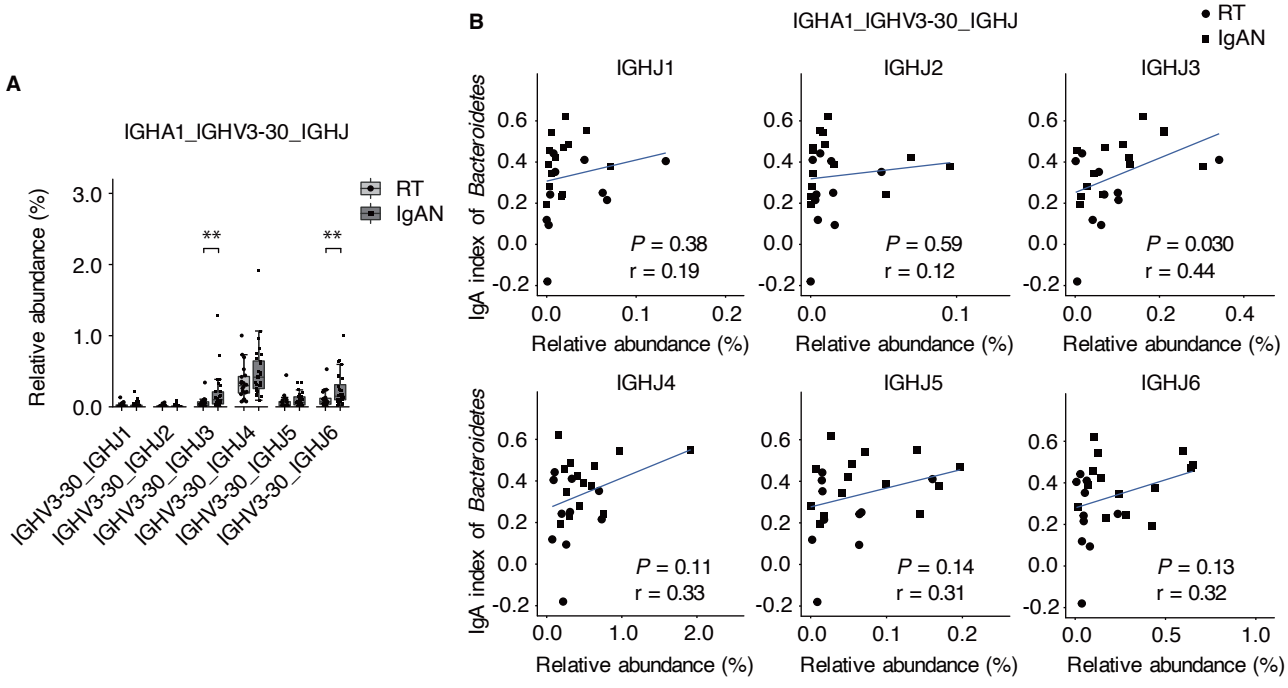

FIGURE S5: Comparison of IGHJ clone in IGHV3-30 with IGHA1 clones between IgAN and RT, and correlation with the IgA index score of the phylum *Bacteroidetes*. (**A**) Relative abundance of IGHA1 with IGHV3-30 and each IGHJ clone for the IgAN (n = 28) and RT (n = 20) groups. Data are presented as median and IQR (*$P < 0.05$, **$P < 0.01$, Mann–Whitney U test). (**B**) Correlation between the relative abundance of IGHA1 with IGHV3-30_IGHJ clones and the IgA index of the phylum *Bacteroidetes* in the patients from both IgAN and RT groups, analyzed by both IgA-SEQ and immunoglobulin repertoire sequencing (n = 24). Correlation of the data was statistically compared using Pearson's correlation and linear regression analysis.

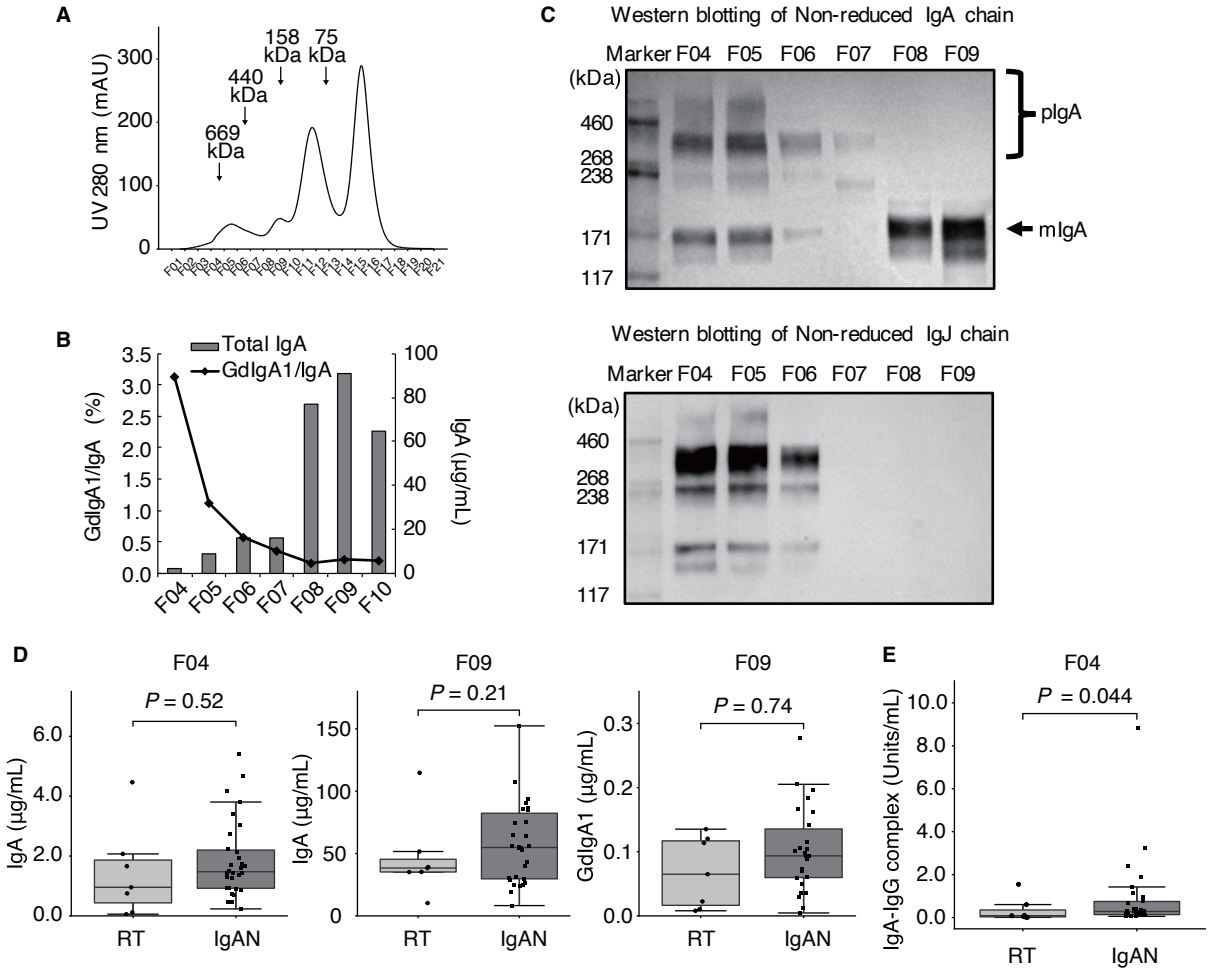

FIGURE S6: Fractionation of IgA complexes from the serum of IgAN or RT patients. (**A**) Sera from IgAN patients were fractionated using gel-filtration chromatography. The chromatograms of a representative IgAN patient, recorded at UV 280 nm; molecular sizes of standard proteins are shown. Each fraction number is shown at the bottom of the figure. (**B**) Concentrations of IgA (bar graph) and GdIgA1/IgA ratio (line graph) in each fraction from a representative IgAN patient. The F04 fraction was evaluated and used as the pIgA fraction, and F09 was evaluated and used as the mIgA fraction. (**C**) Detection of fractionated IgA molecular size (top) and J-chain (bottom) contained in each fraction by immunoblotting using an anti-human IgA alpha-chain antibody and anti-J-chain antibody, respectively, in non-reducing conditions. pIgA (>300 kDa) was only detected in high molecular size fractions. IgAs in the pIgA fraction (F04) contained the J-chain, whereas the mIgA fraction (F09) did not. (**D**) Levels of IgA and GdIgA1 of F04 and F09 fractions. IgA levels in the F04 (left) and F09 (middle) fractions, and GdIgA1 levels in the F09 fraction (right) from IgAN (n = 30) and RT (n = 7) patients. (**E**) Levels of IgA-IgG complexes multiplied by IgA levels in F04 fractions (right) from IgAN (n = 30) and RT (n = 7) patients are shown. The results are shown as optical density (OD) measured at 450 nm. Box plots show the median and IQR, with whiskers of 1.5 × IQR. Data were statistically compared using the Mann–Whitney U test.

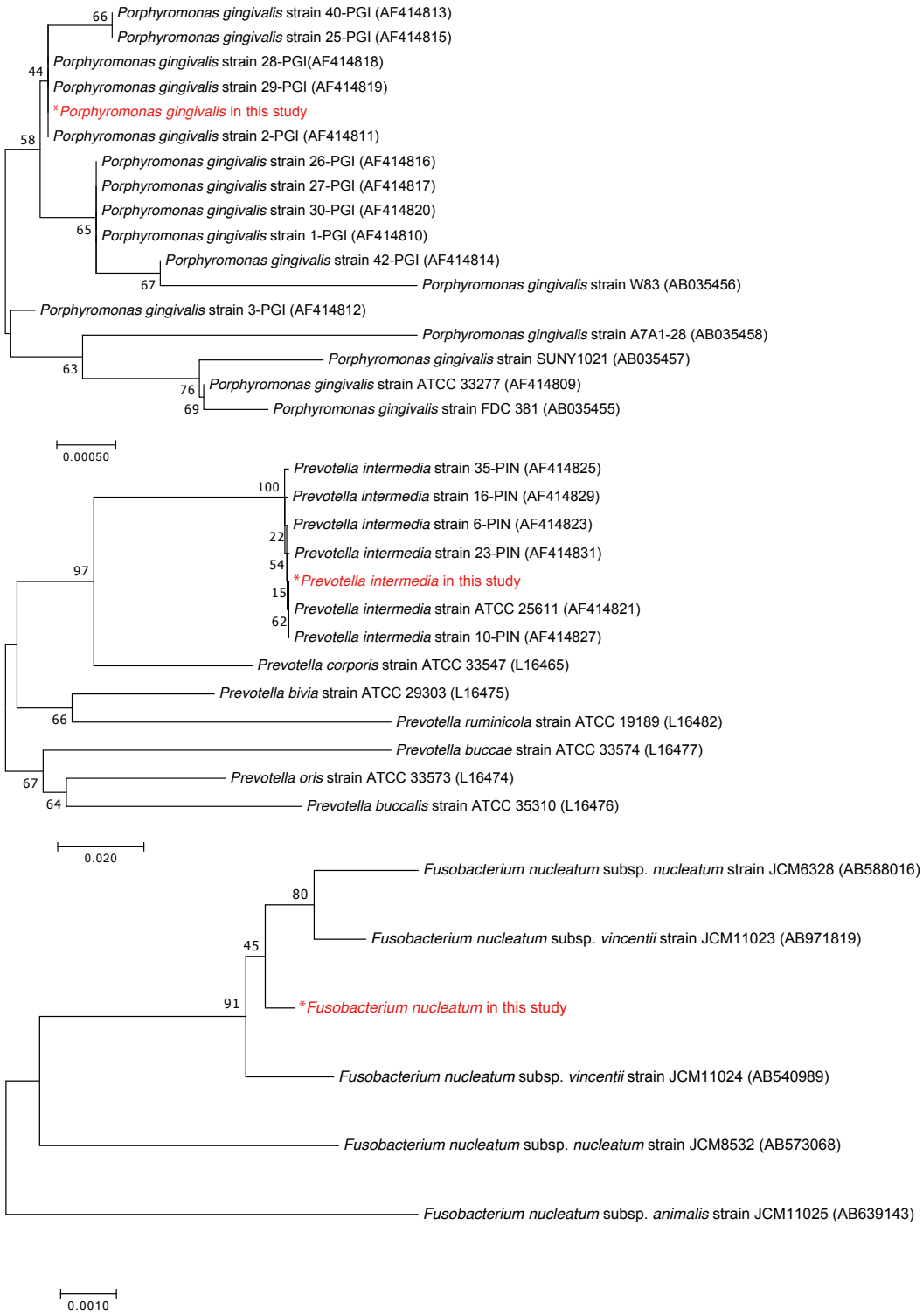

FIGURE S7: Phylogenetic tree of cultured tonsillar bacteria from patients with IgAN generated using nearly full-length sequencing of the 16S rRNA gene. The nearly full-length sequences of the 16S rRNA genes of cultured bacteria from the tonsils were compared with that of each bacterial strain from the DDBJ/EMBL/GenBank database by phylogenetic analysis using MEGA7 software. The constructed phylogenetic trees of *Porphyromonas gingivalis* (top), *Prevotella intermedia* (middle), and *Fusobacterium nucleatum* (bottom) cultured from the tonsils of patients with IgAN are shown. Asterisks indicate the bacterial strains cultured from tonsils in this study. The DDBJ/EMBL/GenBank database bacterial accession numbers are in parentheses. Bootstrap values based on 1000 replicates are shown on the branching point. Scale bar represents substitutions per nucleotide position.

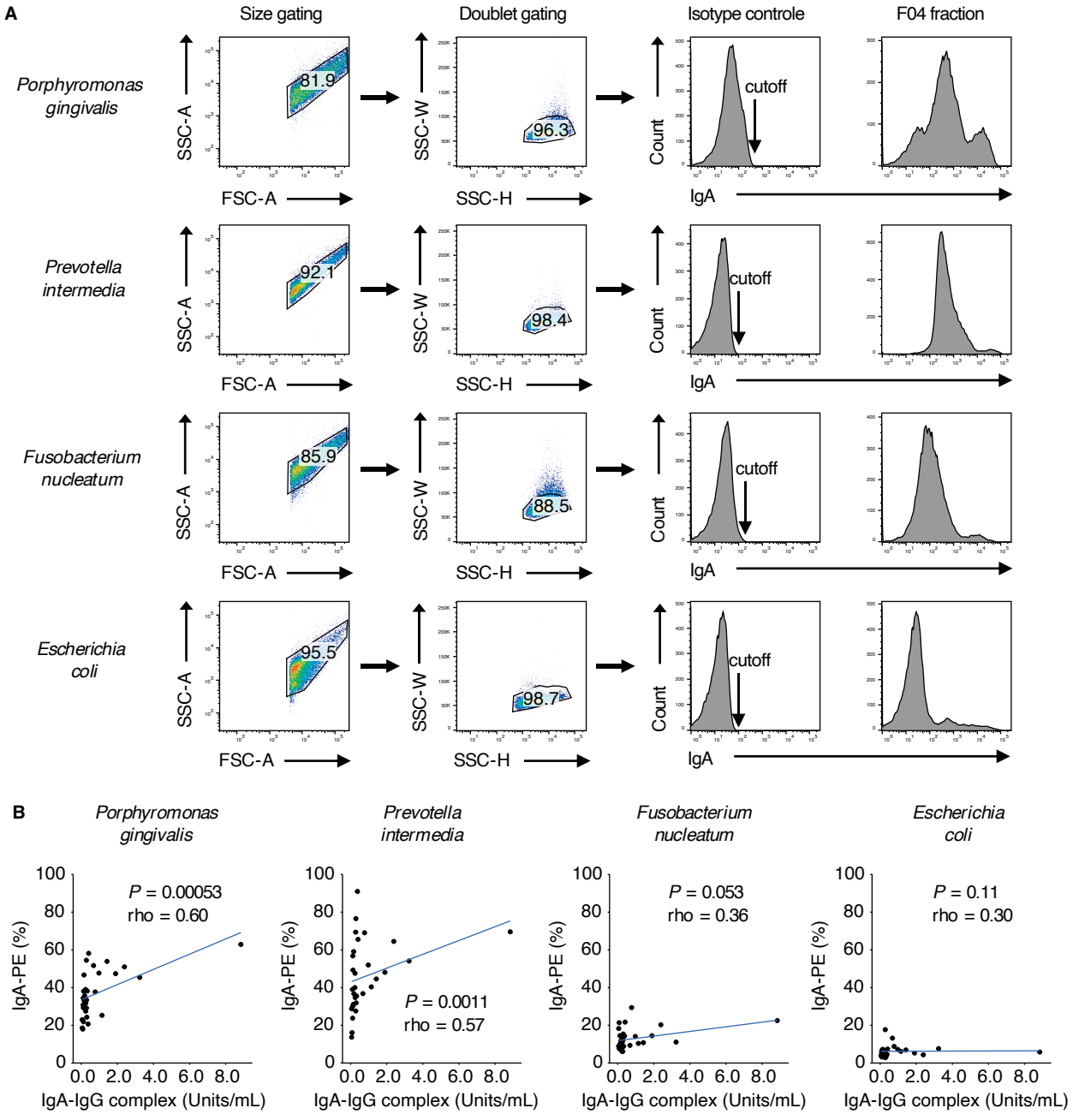

FIGURE S8: Flow cytometric evaluation of IgA binding to cultured bacteria. (**A**) Gating strategy for *Porphyromonas gingivalis*, *Prevotella intermedia*, and *Fusobacterium nucleatum* cultured from the tonsils of IgAN patients and *Escherichia coli* obtained as an ATCC standard strain. The population was first gated using SSC-A and FSC-A. Then, doublet cells were removed before analyzing the fluorescence signal. Samples stained with isotype-control antibody were used to determine the fluorescence intensity corresponding to unspecific binding. Fluorescence intensities greater than the threshold of the isotype control-stained sample were considered as IgA-PE–positive bacteria. (**B**) Correlation between the percent positivity for IgA-PE for each bacterial species and the levels of IgA-IgG complexes multiplied by IgA by F04 fractions in IgAN patients (n = 30). Data were statistically compared using Spearman's correlation and linear regression analysis.

Supplementary data

Aberrant mucosal immunoreaction to tonsillar microbiota in immunoglobulin A nephropathy

Hiroki Yamaguchi, Shin Goto, Nao Takahashi, Masafumi Tsuchida, Hirofumi Watanabe, Suguru Yamamoto, Yoshikatsu Kaneko, Koichi Higashi, Hiroshi Mori, Yukio Nakamura, Arata Horii, Ken Kurokawa, and Ichiei Narita

SUPPLEMENTARY METHODS

Patient samples

IgAN was diagnosed based on pathological findings, such as mesangial IgA deposition by immunofluorescence examination. Tonsillectomy was performed in IgAN patients for clinical remission. No RT patient presented urine abnormalities before enrollment. Exclusion criteria included administration of steroids and/or immunosuppressive agents within the preceding two years, and antimicrobial treatment within two months before tonsillectomy. Tonsillar samples were collected from 2012 to 2018 at Niigata University Hospital and associated facilities. The right palatine tonsils were obtained by tonsillectomy under general anesthesia. Immediately thereafter, the deepest part of the largest crypt (2–3 mm^3 in size) in the upper pole of the tonsil was excised, quickly frozen, and stored at −80 °C. All serum samples were collected immediately before tonsillectomy.

Tonsillar protein extraction and enzyme-linked immunosorbent assay

Tonsillar tissue (30 mg) was suspended in T-PER tissue protein extraction reagent (ThermoScientific, Waltham, MA, USA; cat#78510) and subsequently homogenized using the FastPrep®24 mechanical disruptor (MP Biomedicals, Tokyo, Japan). After centrifugation, the supernatant was collected as total protein solution and quantified using the BCA colorimetric protein assay. The final concentration was set at 1.0 mg/dL. Homogenized tonsils that did not provide sufficient protein for the assay were excluded. APRIL, BAFF, GdIgA1, and IgA concentrations in both the serum and tonsils were measured using the Human APRIL/TNFSF13 DuoSet (R&D

Systems, Minneapolis, MN, USA; cat#DY884B) and the Human BAFF/BLyS/TNFSF13B Quantikine ELISA kit (R&D Systems; cat#DBLYS0B), respectively, according to the manufacturer's protocol. GdIgA1 and IgA concentrations in the tonsil, serum, and in their fractions were measured using the GdIgA1 Assay kit (Immuno-Biological Laboratories, Gunma, Japan, cat#27600) [1] and the Human IgA ELISA Quantitation Set (Bethyl Laboratories, Montgomery, TX, USA; cat#E80-102), respectively. The concentration was determined by reading the absorbance at 450 nm using a microplate reader (Tecan, Männedorf, Switzerland).

IgA-IgG complex levels in fractionated serum were determined by ELISA according to a previous report [2], with minor modifications. Nunc MaxiSorp ELISA plates (Nunc, Roskilde, Denmark) were coated with the $F(ab')_2$ fragment of goat anti-human IgA (1.0 μg/mL, Southern Biotechnology Associates, Birmingham, AL) suspended in 0.05 M carbonate-bicarbonate buffer (pH 9.4). All wells were washed four times with PBS containing 0.05% Tween and 1% BSA. The wells were then incubated with fractionated samples containing 20 ng IgA at room temperature for 1 h. After additional washing, all wells were incubated with HRP-conjugated goat anti-human IgG (1:100,000, Abcam) at room temperature for 1 h and developed with TMB substrate solution. Optical density (OD) values were measured at 450 nm using a microplate reader (Tecan).

Immunohistochemical staining, immunofluorescent staining, and quantitative analysis

We used right tonsillar samples from patients who had undergone tonsillectomy for immunohistochemical staining. The paraffin-embedded sections (3 μm thick) of tonsillectomy samples were deparaffinized in xylene followed by 100% ethanol and rehydrated with graded ethanol. An autoclave was used for heat-based antigen

retrieval in citric acid buffer (pH 6.0) for APRIL staining, whereas proteolytic-induced antigen retrieval was performed by incubation with proteinase K (Dako, Carpinteria, CA, USA; cat#S3020) at room temperature for 5 min for BAFF staining. After blocking with peroxidase blocking solution (Dako) and background-reducing components, slides were incubated with a mouse anti-APRIL/TNFSF13 monoclonal antibody (10 μg/mL, Aprily-8; Novus Biologicals, Littleton, CO, USA) or a rat anti-human BAFF monoclonal antibody (1:250; Buffy-2, Abcam, Cambridge, UK) overnight. Slides were then incubated with horseradish peroxidase (HRP)-conjugated anti-mouse secondary antibodies (EnVision$^+$ Systems; Dako; cat#K4000) or HRP-conjugated rabbit anti-rat immunoglobulins (1:100; Dako; cat#P0450) at room temperature for 1 h, respectively. Reaction products were visualized using 3,3′-diaminobenzidine.

For immunofluorescence staining, the paraffin-embedded sections of kidney biopsy samples from patients with IgAN were prepared at a thickness of 3 μm. The methods of deparaffinization, blocking, washing, and antibody dilution were the same as those used for immunohistochemical staining. We used 0.05% bacterial protease subtilisin A (Sigma-Aldrich, St Louis, MO) at room temperature for antigen retrieval. Slides were incubated with a rat anti-GdIgA1 monoclonal antibody (100 μg/mL; KM55, Immuno-Biological Laboratories) at 4 °C overnight, washed, then incubated with FITC-conjugated goat anti-rat IgG antibody (1;100; Sigma-Aldrich) at room temperature for 1 h. Slides were then washed and mounted in Vectashield with 4,6-diamidino-2-phenylindole (DAPI) (Vector Laboratories, Burlingame, CA). Images were acquired using a confocal laser scanning microscope (Fluoview FV1000, Olympus, Tokyo, Japan).

The proportion of the area stained with immunofluorescence antibody was quantified using ImageJ software

(http://www.rsb.info.nih.gov/ij/), and its distribution was ascertained using Fiji [3], as per previous studies [4-6]. First, we photographed stained glomerular images at 40x magnification (TIFF file) in single biopsy sections and measured the area of each glomerulus using ImageJ. Subsequently, using the "Split channel" tools, the immunofluorescence-stained glomerular image was evaluated and divided into green, red, and blue-stained areas. Finally, we quantified the FITC positively stained area using the "Threshold" tool and calculated the proportion of positively stained area per glomerulus. We evaluated > 5 glomeruli in each sample and calculated the mean values of the proportion of immunostained area per glomerulus.

Bacterial sorting for IgA-SEQ

Bacterial sorting was performed according to a previous report [7] and applied to tonsillar samples with some modifications. First, 30 mg of each tonsillar sample was suspended in 1 mL phosphate buffered saline (PBS). The supernatants were centrifuged, and bacterial pellets were collected and washed with 1 mL staining buffer [PBS containing 1% (w/v) bovine serum albumin]. Samples were then blocked with 100 μL staining buffer containing 20% mouse serum. After washing and suspending with 1 mL staining buffer, we divided bacterial suspensions into 900 and 100 μL aliquots. Bacterial pellets from 100 μL bacterial suspensions were incubated with 100 μL staining buffer containing the mouse IgG1-PE isotype (Miltenyi Biotec, Bergisch Gladbach, Germany; cat#130-092-212), and were saved as the isotype-control-stained sample for FACS analysis. Bacterial pellets from 900 μL bacterial suspensions were incubated with staining buffer containing PE-conjugated mouse anti-human IgA (IS11-8E10, Miltenyi Biotec). Anti-IgA-stained bacterial samples were washed thrice with 1 mL sterilized MACS buffer

[PBS containing 1% (w/v) bovine serum albumin and 2 mmol EDTA] and incubated with anti-PE Microbeads (Miltenyi Biotec; cat#130-048-801). After washing, manual MACS was carried out on LS-columns. Following MACS separation, both the IgA-binding and IgA-non-binding fractions were sorted using FACSAria II (BD Biosciences, Tokyo, Japan), and data were analyzed using FlowJo software (Treestar, Ashland, OR, USA). The gating strategy for IgA-SEQ is described detail in Supplementary data, Figure S2A. Overall, >100,000 events were collected from the IgA-positive fraction from each sample.

Bacterial 16S rRNA gene amplification

Genomic DNA from tonsillar crypts and sorted fractions was extracted using the PowerSoil DNA Isolation Kit (Qiagen, Hilden, Germany; cat#12888). We amplified the bacterial 16S rRNA V4 genes for PCR amplification of genomic DNA (1 ng) using the primer set 515F/806R modified with Illumina adaptors, as follows: 515F, 5′-TCGTCGGCAGCGTCAGATGTGTATAAGAGACAGGTGYCAGCMGCCGCGGTAA-3′ and 806R 5′-GTCTCGTGGGCTCGGAGATGTGTATAAGAGACAGGACTACHVGGGTATCTAATCC-3′ [8]. PCR was performed using KOD Plus Ver.2 DNA polymerase (Toyobo, Osaka, Japan; cat#KOD-211), and PCR cycling conditions were as follows: 98 °C for 2 min; 35 cycles each of 98 °C for 10 s, 56 °C for 30 s, and 68 °C for 1 min; and 68 °C for 7 min. PCR amplicons were purified using AMPure XP magnetic purification beads (Beckman Coulter, Brea, CA, USA; cat#A63880), and then index sequences were added by amplification with Nextera XT Index Kit v2 (Illumina, San Diego, CA, USA; cat#FC-131-2001). Indexed amplicon products were quantified using a Qubit 3.0 Fluorometer (ThermoScientific). Mixed samples were prepared by pooling equal

amounts of the PCR amplicons from each sample. Samples were sequenced using an Illumina MiSeq system with the 2 x 251 base-pair paired-end protocol.

Taxonomic classification

Sequence data analysis of the 16S rRNA gene amplicon was performed using the open-source QIIME2 pipeline version 2018.4 [9]. Demultiplexed FASTQ.gz files were subjected to quality filtering, de-noising, trimming of primers, truncation of length, pair-end merging, and discarding chimeric reads using the DADA2 plugin [10], as processed by the qiime dada2 denoise-paired command to obtain features that comprised essentially any unit of observation. Consequently, a feature table was extracted. Taxonomic classification of the features was performed using the QIIME2 "q2-feature-classifier" plugin [11] with the Greengenes 13.8. 99% operational taxonomic units (OTUs) full-length sequences database [12]. Taxonomic composition or relative abundance of bacterial phyla and genera were calculated using the QIIME2 taxa barplot command. Alpha-diversity analyses by observed OTUs were performed using the "q2-diversity" plugin of QIIME2 at a sampling depth of 7500. Differences in bacterial composition were statistically analyzed via permutational ANOVA using R (https://www.r-project.org) in conjunction with the "vegan" package, with 9999 permutations based on the Bray–Curtis dissimilarity index.

IgA index analysis

The IgA index was calculated using the relative abundance of bacterial phyla and genera for the IgA-positive

(IgA$^+$) and IgA-negative fractions (IgA$^-$), as previously reported [13]. We first excluded bacterial phyla and genera whose relative abundance was <0.001 in the pre-sort sample, and then added a pseudocount (= 0.001) to every detected bacterial phylum and genus [14]. The relative abundance of the bacterial phyla and genera, given the pseudocount, was log-transformed and calculated for the IgA index to compare the significance of the differences in the bacterial abundances of the IgA$^+$ and IgA$^-$ fractions, as follows:

$$IgA\ index = -\frac{\{log(IgA^+) - log(IgA^-)\}}{\{log(IgA^+) + log(IgA^-)\}}.$$

Adaptor-ligation PCR and high-throughput amplicon sequencing

Adaptor-ligation PCR and primer setting (Table S2) were performed according to a previous report [15], with some modifications. Total RNA (30 mg) of each dissected tonsillar sample was extracted using the RNeasy Plus Universal Mini Kit (Qiagen; cat#73404). RNA purity was measured using the Agilent 2100 Bioanalyzer. RNAs with integrated number of >5.0 were considered to be of good quality, and were selected for further analysis. Total RNA (2 μg) was converted to cDNA using PrimeScript Reverse Transcriptase (TaKaRa, Shiga, Japan; cat#2680A) and primed with a BSL-18E primer containing poly(dT) 18 and a NotI restriction site. After cDNA synthesis, double-stranded (ds)-cDNA was synthesized with *Escherichia coli* DNA polymerase I in the presence of both *E. coli* DNA ligase and ribonuclease H, and the ds-cDNA was blunted using T4 DNA polymerase. The ds-cDNA was ligated with a P10EA/P20EA adaptor and cut with NotI. After cleaning up the reaction, first and nested PCR

using primers specific to both the P20EA and C-region of the IgA heavy chain (CA1 and CA2, respectively) was conducted. The both first and nested PCR conditions were as follows: 20 cycles of 95°C for 20 s, 65°C for 30 s, and 72°C for 1 min. PCR amplicons were prepared by amplification of the nested PCR products using P20EA-ST1-R and C-region-specific Tag primer (CA-ST1-R), and then purified using AMPure XP magnetic purification beads. After purification, index sequences were added by amplification with the Nextera XT Index Kit v2. Equal amounts of PCR amplicons were subjected to sequencing using Illumina MiSeq with the 2 × 301 base-pair paired-end protocol.

Bioinformatics for immunoglobulin sequencing

To detect the distributions of IGHV, IGHD, IGHJ, and IGHC gene segments and the deduced CDR3 amino acid sequence of tonsillar IgA, sequence reads were analyzed using the bioinformatics software developed by Repertoire Genesis Incorporation (Ibaraki, Japan) [15, 16]. The V, D, J, and C segments of IGH were discriminated using reference sequence data sets available from the IMGT database (http://www.imgt.org). The Repertoire Genesis software automatically performed data processing, assignment of unique sequence reads, and data aggregation. Only unique reads were used for both determination of the V, D, and J genes and for deducing the amino acid sequences of CDR3. Relative abundance of in-frame reads in each sample were calculated and used for further analysis.

Size fractionation

An aliquot (200 μL) of serum was diluted in PBS (pH 7.4), filtered, and separated by gel filtration through a Superdex 200 10/300 column connected to a liquid chromatography system (AKTA Pure 25L) controlled with Unicorn 7.1 (GE Healthcare, Buckinghamshire, UK). Molecular weight was determined using the Gel Filtration Calibration Kit HMW (GE Healthcare; cat#28403842). Fractions of 500 μL were collected and analyzed.

Western blotting

Fractionated samples containing 20 ng IgA were subjected to electrophoresis under non-reducing conditions in a 3–8% Tris-acetate gel electroblotted onto polyvinylidene fluoride membranes. After blocking, for the detection of IgA, membranes were incubated with horseradish peroxidase-conjugated goat anti-human IgA alpha chain (1:15 000; Abcam, Cambridge, UK; cat#ab97215). For detection of the J-chain, membranes were incubated with rabbit anti-human IGJ antibody (1:500; Proteintech, Chicago, IL, USA; cat#13688-1-AP) and mouse horseradish peroxidase-conjugated anti-rabbit IgG antibody (1:1000; Santa Cruz, Dallas, TX, USA; cat#sc-2357). Blots were developed and target protein bands were detected using the Lumino Graph (ATTO, Tokyo, Japan).

Bacterial culture

Dissected tonsils were homogenized, suspended in 1 mL normal saline, and anaerobically subcultured on Brucella HK agar for 7 days. The bacterial strains were identified using the RapID ANA II System (Amco, Tokyo, Japan; cat#551-63803-5). *Porphyromonas gingivalis*, *Prevotella intermedia*, and *Fusobacterium nucleatum* colonies were picked and inoculated in Gifu Anaerobic Media broth and cultured at 37 °C for 72 h in anaerobic

conditions. *Escherichia coli* (ATCC 25922) strains were purchased from MicroBiologics CE, inoculated in Luria–Bertani broth, and cultured at 37 °C overnight. Cultured bacteria were centrifuged, and bacterial pellets were collected and washed with PBS.

Nearly full-length sequencing of the 16S rRNA gene

Genomic DNA was extracted from cultured bacteria using the PowerSoil DNA Isolation Kit, and the nearly full-length 16S rRNA genes were amplified by PCR using the following primers: 27F, 5'-AGAGTTTGATCCTGGCTCAG-3′, and 1492R, 5'-GGCTACCTTGTTACGACTT-3′ [17]. PCR reactions were performed with TaKaRa Ex Taq (cat#RR001A) under the following cycling conditions: 94 °C for 3 min; 30 cycles each of 94 °C for 30 s, 55 °C for 1 min, and 72 °C for 1 min; and 72 °C for 7 min. PCR amplicons were sequenced using the BigDye Terminator v1.1 Cycle Sequencing Kit on an Applied Biosystems 3130xl Genetic Analyzer. We obtained the sequences of the 16S rRNA gene of each bacterial strain from the DDBJ/EMBL/GenBank database and performed multiple sequence alignments using the CLUSTAL W program [18]. We constructed and visualized the phylogenetic trees with MEGA7 software [19] using the neighbor-joining method with a bootstrap of 1000 replicates.

Flow cytometry: IgA binding to cultured strains

IgA binding to bacteria was evaluated using flow cytometry as previously described, with minor modifications [20, 21]. Cultured bacteria were suspended in PBS, and 2.0×10^6 bacteria were washed with 1 mL staining buffer.

Then, pelleted bacteria were incubated with 50 μL of the F04 or F09 fraction at 4 °C overnight. The IgA concentrations of the F09 fractions of each sample were adjusted to that of the F04 fraction before incubation. After washing, incubated bacteria were stained with PE-conjugated mouse anti-human IgA monoclonal antibody or mouse IgG1-PE isotype and saved as IgA-binding samples and control samples, respectively, for flow cytometric analysis on a FACSAria II. The gating strategy for each strain is described detail in Supplementary data, Figure S8.

TABLE S1: Characteristics of enrolled patients used for serum analysis.

Patient characteristics	**IgAN** **n = 30**	**RT** **n = 7**	***P*-value**
Age (years)	33.9 ± 10.8	35.1 ± 14.7	0.799
Sex (male)	11 (35.5)	3 (42.9)	1.000
BMI (kg/m^2)	21.6 ± 2.4	23.9 ± 6.3	0.115
Systolic BP (mmHg)	118.4 ± 12.8	113.0 ± 20.1	0.372
Diastolic BP (mmHg)	71.9 ± 9.3	73.3 ± 12.6	0.741
s-Cre (mg/dL)	0.82 ± 0.27	0.7 ± 0.2	0.213
eGFR (mL/min/1.73m^2)	80.4 ± 21.5	96.4 ± 24.6	0.094
BUN (mg/mL)	14.0 ± 5.0	13.3 ± 3.4	0.724
TP (g/dL)	7.2 ± 0.5	7.3 ± 0.7	0.558
UA (mg/dL)	5.1 ± 0.9	5.3 ± 1.2	0.643
C3 (mg/dL)	94.5 ± 19.2	-	-
Urinary protein (g/gCr)	0.40 (0.20, 0.70)	-	-
Period from renal biopsy to tonsillectomy (day)	187 (124, 368)	-	-
RASI	20 (66.7)	1 (14.3)	<0.001
Oxford classification			
Mesangial hypercellularity (M0/M1)	20/10		
Endocapillary hypercellularity (E0/E1)	12/18		
Segmental glomerulosclerosis (S0/S1)	5/25		
Tubular atrophy/interstitial fibrosis (T0/T1/T2)	28/2/0		
Crescents (C0/C1/C2)	11/19/0		

BMI, body mass index; BP, blood pressure; s-Cre, serum creatinine; eGFR, estimated glomerular filtration rate; BUN, blood urea nitrogen; TP, total protein; UA, uric acid; C3, complement component 3; RASI, renin angiotensin aldosterone system inhibitor. Data are presented as the means ± standard deviation, median (IQR), or number (ratio) and were statistically compared using Student's *t*-test or Fisher's exact test. RASI were significantly higher in patients with IgAN as compared to those with RT.

TABLE S2: Primers for adaptor-ligation PCR and immunoglobulin sequencing of tonsillar IgA heavy chain.

Primers	**Sequence**
BSL-18E	AAAGCGGCCGCATGCTTTTTTTTTTTTTTTTTVN
P20EA	TAATACGACTCCGAATTCCC
P10EA	GGGAATTCGG
P22EA-ST1-R	GTCTCGTGGGCTCGGAGATGTGTATAAGAGACAGCTAATACGACTCCGAATTCCC
CA1	GCTGGCTGCTCGTGGTGTAC
CA2	GGGAAGTTTCTGGCGGTCACG
CA-ST1-R	TCGTCGGCAGCGTCAGATGTGTATAAGAGACAGGGGGGAAGAAGCCCTGGACCA

REFERENCES

1. Yasutake J, Suzuki Y, Suzuki H et al. Novel lectin-independent approach to detect galactose-deficient IgA1 in IgA nephropathy. *Nephrol Dial Transplant* 2015; 30: 1315–1321.

2. Matousovic K, Novak J, Yanagihara T et al. IgA-containing immune complexes in the urine of IgA nephropathy patients. *Nephrol Dial Transplant* 2006; 21: 2478–2484.

3. Schindelin J, Arganda-Carreras I, Frise E et al. Fiji: an open-source platform for biological-image analysis. *Nat Methods* 2012; 9: 676–682.

4. Prasad K, Prabhu GK. Image analysis tools for evaluation of microscopic views of immunohistochemically stained specimen in medical research–a review. *J Med Syst* 2011; 36: 2621–2631.

5. Jensen EC. Quantitative analysis of histological staining and fluorescence using ImageJ. *Anat Rec (Hoboken)* 2013; 296: 378–381.

6. Oruc Z, Oblet C, Boumediene A et al. IgA structure variations associate with immune stimulations and IgA mesangial deposition. *J Am Soc Nephrol* 2016; 27: 2748–2761.

7. Palm NW, de Zoete MR, Cullen TW et al. Immunoglobulin A coating identifies colitogenic bacteria in inflammatory bowel disease. *Cell* 2014; 158: 1000–1010.

8. Caporaso JG, Lauber CL, Walters WA et al. Global patterns of 16S rRNA diversity at a depth of millions of sequences per sample. *Proc Natl Acad Sci U.S.A.* 2011; 108: 4516–4522.

9. Caporaso JG, Kuczynski J, Stombaugh J et al. QIIME allows analysis of high-throughput community sequencing data. *Nat Methods* 2010; 7(5): 335–336.

10. Callahan BJ, McMurdie PJ, Rosen MJ et al. DADA2: High-resolution sample inference from Illumina amplicon data. *Nat Methods* 2016; 13: 581–583.

11. Bokulich NA, Kaehler BD, Rideout JR et al. Optimizing taxonomic classification of marker-gene amplicon sequences with QIIME 2's q2-feature-classifier plugin. *Microbiome* 2018; 6: 90.

12. McDonald D, Price MN, Goodrich J et al. An improved Greengenes taxonomy with explicit ranks for ecological and evolutionary analyses of bacteria and archaea. *ISME J* 2012; 6: 610–618.

13. Kau AL, Planer JD, Liu J et al. Functional characterization of IgA-targeted bacterial taxa from undernourished Malawian children that produce diet-dependent enteropathy. *Sci Transl Med* 2015; 7: 276ra24.

14. Viladomiu M, Kivolowitz C, Abdulhamid A et al. IgA-coated *E. coli* enriched in Crohn's disease spondyloarthritis promote T_H17-dependent inflammation. *Sci Transl Med* 2017; 9: eaaf9655.

15. Kitaura K, Yamashita H, Ayabe H et al. Different somatic hypermutation levels among antibody subclasses disclosed by a new next-generation sequencing-based antibody repertoire analysis. *Front Immunol* 2017; 8:389.

16. Ichinohe T, Miyama T, Kawase T et al. Next-generation immune repertoire sequencing as a clue to elucidate the landscape of immune modulation by host–gut microbiome interactions. *Front Immunol* 2018; 9:668.

17. Weisburg WG, Barns SM, Pelletier DA, Lane DJ. 16S ribosomal DNA amplification for phylogenetic study. *J Bacteriol* 1991; 173: 697–703.

18. Thompson JD, Higgins DG, Gibson TJ. CLUSTAL W: improving the sensitivity of progressive multiple sequence alignment through sequence weighting, position-specific gap penalties and weight matrix choice. *Nucleic Acids Res* 1994; 22: 4673–4680.

19. Kumar S, Stecher G, Tamura K. MEGA7: Molecular evolutionary genetics analysis version 7.0 for bigger datasets. *Mol Biol Evol* 2016; 33: 1870–1874.

20. McCarthy DD, Kujawa J, Wilson C et al. Mice overexpressing BAFF develop a commensal flora–dependent, IgA-associated nephropathy. *J Clin Invest* 2011; 121: 3991–4002.

21. Slack E, Hapfelmeier S, Stecher B et al. Innate and adaptive immunity cooperate flexibly to maintain host-microbiota mutualism. *Science* 2009; 325: 617–620.